Clinical Science (2023) **137** 195–217
https://doi.org/10.1042/CS20220654

PORTLAND PRESS

Research Article

Increased β1-adrenergic receptor antibody confers a vulnerable substrate for atrial fibrillation via mediating Ca^{2+} mishandling and atrial fibrosis in active immunization rabbit models

Huaxin Sun[1,2,*], Jie Song[1,2,*], Kai Li[1,2,*], Yao Li[3], Luxiang Shang[4], Qina Zhou[5], Yanmei Lu[1,2], Yazhen Zong[1,2], Xiuyuan He[1,2], Muzappar Kari[1,2], Hang Yang[1,2], Xianhui Zhou[1,2], Ling Zhang[1] and Baopeng Tang[1,2]

[1]Xinjiang Key Laboratory of Cardiac Electrophysiology and Remodeling, The First Affiliated Hospital of Xinjiang Medical University, Urumqi 830011, China; [2]Department of Pacing and Electrophysiology, The First Affiliated Hospital of Xinjiang Medical University, Urumqi 830011, China; [3]Psychosomatic Medical Center, The Fourth People's Hospital of Chengdu, Chengdu, China; [4]Department of Cardiology, The First Affiliated Hospital of Shandong First Medical University and Shandong Provincial Qianfoshan Hospital, Shandong Medicine and Health Key Laboratory of Cardiac Electrophysiology and Arrhythmia, Jinan, China; [5]School of Nursing, Midwifery and Social Work, University of Queensland, Brisbane, Queensland, Australia

Correspondence: Baopeng Tang (tangbaopeng1111@163.com) or Ling Zhang (ydzhangling@126.com) or Xianhui Zhou (zhouxhuiyf@163.com)

Background: Autoimmune disorder is the emerging mechanism of atrial fibrillation (AF). The β1-adrenergic receptor antibody (β1-AAb) is associated with AF progress. Our study aims to investigate whether β1-AAbs involves in atrial vulnerable substrate by mediating Ca^{2+} mishandling and atrial fibrosis in autoimmune associated AF. Methods: Active immunization models were established via subcutaneous injection of the second extracellular loop (ECL2) peptide for β1 adrenergic receptor (β1AR). Invasive electrophysiologic study and *ex vivo* optical mapping were used to evaluate the changed electrophysiology parameters and calcium handling properties. Phospho-proteomics combined with molecular biology assay were performed to identify the potential mechanisms of remodeled atrial substrate elicited by β1-AAbs. Exogenous β1-AAbs were used to induce the cellular phenotypes of HL-1 cells and atrial fibroblasts to AF propensity. Results: β1-AAbs aggravated the atrial electrical instability and atrial fibrosis. Bisoprolol alleviated the alterations of action potential duration (APD), Ca^{2+} transient duration (CaD), and conduction heterogeneity challenged by β1-AAbs. β1-AAbs prolonged calcium transient refractoriness and promoted arrhythmogenic atrial alternans and spatially discordant alternans, which were partly counteracted through blocking β1AR. Its underlying mechanisms are related to β1AR-drived CaMKII/RyR2 activation of atrial cardiomyocytes and the myofibroblasts phenotype formation of fibroblasts. Conclusion: Suppressing β1-AAbs effectively protects the atrial vulnerable substrate by ameliorating intracellular Ca^{2+} mishandling and atrial fibrosis, preventing the process of the autoimmune associated AF.

[*]These authors contributed equally to this work.

Received: 08 October 2022
Revised: 19 December 2022
Accepted: 03 January 2023

Accepted Manuscript online: 04 January 2023
Version of Record published: 27 January 2023

Introduction

Atrial fibrillation (AF) is a global epidemic of cardiac arrhythmia with increased morbidity, disability rate and mortality, imposing a severe economic and social burden [1]. The pathogenesis of miscellaneous AF is attributed to different pathophysiological mechanisms that embrace electrical remodeling, structural remodeling, autonomic dysfunction and oxidative stress [2]. Autoimmune mechanisms, an emerging

Clinical Science (2023) **137** 195–217
https://doi.org/10.1042/CS20220654

field, are implicated in arrhythmogenesis [3]. Hence, many cases of AF subsets with organ-specific autoimmune comorbidities such as hypothyroidism, systemic lupus erythematosus (SLE) and Type 2 diabetes are at risk of higher hospitalization rates and worse outcomes with age [4,5,6].

Autoantibodies are the byproduct of the derailment of adaptive immune system to combat autoimmunity in the pathologic conditions [7]. The β1-adrenergic receptor antibody (β1-AAb), a well-known autoantibody in the cardiovascular system, targets the functional domain on the second extracellular loop of the β1-adrenergic receptor (β1AR) and modulates these receptor's activities [8]. Initially, β1-AAbs are detected in many structural heart diseases, especially in dilated cardiomyopathy or Chagas' disease [9]. With the developing studies, the higher titers of β1-AAbs are detected in approximately 50% of patients with atrial and ventricular arrhythmias [10,11,12]. Our recent work substantiated that elevated β1-AAbs positively correlate with left atrial diameters in paroxysmal AF patients and exacerbate the atrial fibrosis [13]. Accumulating evidence from basic experiments supported the contributions of β1-AAbs in arrhythmia susceptibilities through promoting numerous adverse cardiac phenotypes, including apoptosis, autophagy, and vulnerable electrophysiologic properties [14,15,16]. Nevertheless, precise pathophysiologic and molecular mechanisms of β1-AAbs engaged in AF remains obscure.

Calcium influx and efflux coordinate electrophysiological signaling and contraction consistency in the physiologic state [17]. Ca^{2+} handling is an inherent capability of cardiomyocytes to ensure a dynamic calcium balance between the sarcoplasmic reticulum (SR) and cytoplasm, favoring the intracytoplasmic Ca^{2+} activity initiated by the calcium-induced calcium release process [18]. Ca^{2+} handling abnormality has been considered the hallmark of atrial remodeling through facilitating AF triggers and creating substrate [19]. In terms of the trigger, SR Ca^{2+} mishandling lights the calcium sparks to propagate calcium waves, evokes calcium transient and sequentially induces delayed after depolarizations (DADs) [20]. Regarding substrate, Ca^{2+} mishandling promotes action potential duration (APD) alterations in a calcium-mediated $I_{ca(L)}$ inactivation manner. Moreover, enhanced calcium contents in SR caused by Ca^{2+} mishandling enable the excessive response to extra stimuli such as burst pacing or triggered impulse [21].

According to our knowledge, Ca^{2+} release from SR is partly determined by adrenergic signaling due to the increased function of the ryanodine receptor (RyR2) with phosphorylated modification [22]. In contrast with isoprenaline (ISO), a common β1-AR agonist, β1-AAb, produces a longer receptor activation effect in cardiac hypertrophy [10]. Crucially, β1-AAb mediates the desensitization of β1-AR and relies on the restrictions of receptor endocytosis scaffold protein β-arrestin1/2 in HL-1 cells, implying that β1-AAb may act as a distinct driver of β1-AR signaling in cardiac arrhythmia [23]. The β1-AAb regulation link to Ca^{2+} handling is unclear till now. We aim to investigate whether β1-AAb is involved in AF substrate formation and atrial remodeling in the active immunization rabbit models and its potential molecular mechanisms.

Methods

Animal preparation and study protocol

Twenty-six New Zealand white rabbits (weighing 2.5–3.5 kg) were purchased from the Animal Laboratory Center of Xinjiang Medical University. All animal experiments were taken place at the Xinjiang key laboratory of cardiac electrophysiology and remodeling of First affiliated hospital of Xinjiang Medical University.

Before the model construction, a random number table was applied for the first randomization (control group, n=10; β1-AAb group, n=8; and bisoprolol group, n=8). The active immunization model was established by manually injecting of the second extracellular loop (ECL2) peptide for β1AR (a conserved amino acid sequence as ^{197}HWWRAESDEARRCYNDPKCCDFVTNR^{223}) [24,13]. For the first injection, 2 mg of β1AR-ECL2 was dissolved in 1 mL of the complete Freund's adjuvant (Sigma-Aldrich, St. Louis, MO, U.S.A.) and injected subcutaneously four or five locations around the paravertebral region. Subsequent injections of β1AR-ECL2 were mixed in incomplete Freund's adjuvant, and the same method above was repeated three times. The interval between every two injections was 2 weeks (Figure 1A). Animals in the control group received only equal vehicle injections without β1AR-ECL2 [24,13]. Venous blood was extracted from the ear vein before each injection, and β1-AAb titers were detected from blood samples using an enzyme-linked immunosorbent assay (ELISA). All rabbits with positive β1-AAb titers were chosen for the following study (control group: n=7; β1-AAb group, n=7; and bisoprolol group, n=7) [24,25]. Bisoprolol (Merck Inc., Germany), a selective β1AR blocker, was employed to resist β1AAb-induced biological effects. Bisoprolol was administered orally to subjects at a dose of 2 mg/kg per day for 2 weeks [26].

Electrophysiologic measurement *in vivo*

The invasive operation on animals was carried out under anesthesia. Anesthesia was induced with 0.2 ml of Zoletil 50 (Virbac S.A., France) and 0.2 ml of xylazine (Huamu Animal Health Care Products Co., Ltd., China) and maintained

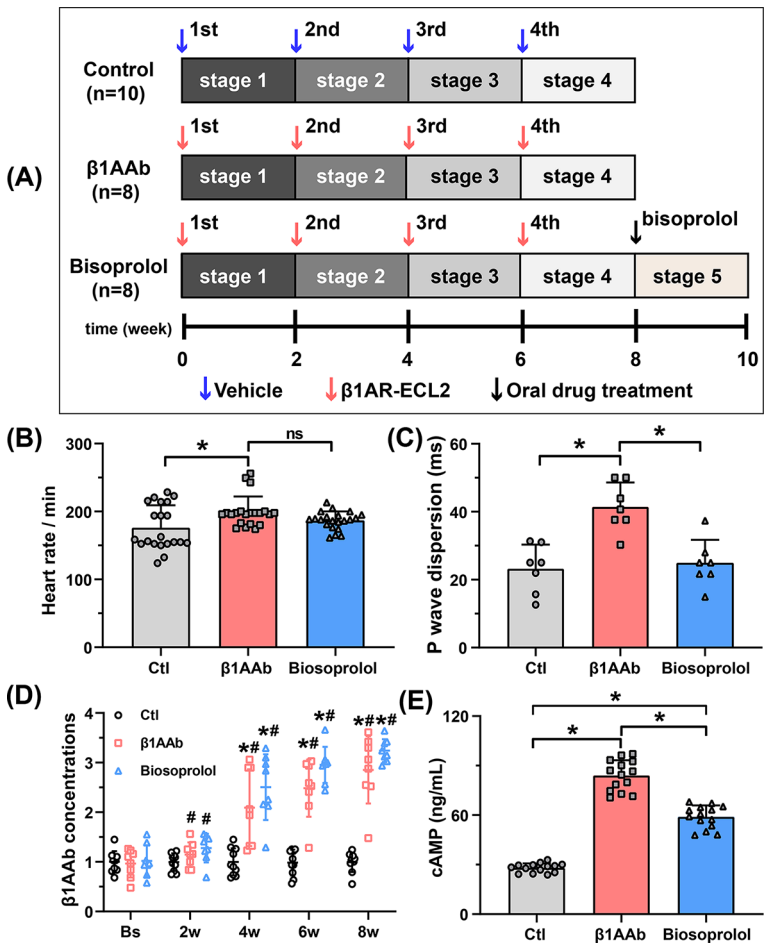

Figure 1. Study protocol and Establishments of active immunization models

(**A**) Study protocol. ECL2 was injected at four time points and per stage persisted 2 weeks (control group, n=10; β1-AAb group, n=8; bisoprolol group, n=8). Bisoprolol was administered after 8-week active immunization for 2 weeks. Seven animal models per group were chosen for the next experiments. (**B**) Heart rate monitoring of three groups at the end point of each *in vivo* experiment (n=7) per group. (**C**) calculation of P wave dispersion from ECG results (n=7) per group. (**D**) Plasma β1-AAb concentrations of three groups at five time points, (n=7) per group, $^{*}P<0.05$ vs. baseline of each group at different time points; $^{\#}P<0.05$ vs. control group at same time points among different groups. (**E**) Detection of atrial cAMP contents of three groups after extracting atrial tissues, (n=7) per group. $^{*}P<0.05$ as indicated, and ns indicates no significance.

with sodium pentobarbital (3 mg/100 ml). Ear venous access was set for intraoperative rehydration. A 5-min electrocardiogram monitoring (ECG) was carried out using a Lead-7000 device (Jinjiang Electronic Science and Technology Inc., Chengdu, China). Surface ECG parameters were calculated manually from four limb leads. After adequately exposing the unilateral jugular vein, a 4-French vascular sheath and a 4-French 10-pole electrode were sequentially placed into the venous system to reach the high right atrium site. Electrophysiologic parameters were measured in our previous work [27]. Atrial effective refractory period (AERP) was examined in S1-S2 mode (eight S1 programmed stimuli with an advanced S2 stimulus, S1S1 interval = 200 ms, width = 0.5 ms), while AF inducibility was measured in S1-S1 mode (burst pacing at 4 V for 10 s, S1S1 interval = 50 ms). AF was described as the rapid atrial arrhythmia with the f wave and absolute irregular RR interval. The window of vulnerability (WOV) was defined as the difference value between the largest and smallest S1-S2 interval when exerting AERP detection. AF inducibility was a proportion that AF occurrences versus total induction times in each animal. AF duration was calculated by the accumulated AF episodes after ten burst pacing per animal. All animals were performed euthanasia by injecting overdose sodium pentobarbital through the ear venous access at the end of experiment.

Clinical Science (2023) **137** 195–217
https://doi.org/10.1042/CS20220654

Echocardiography

All animals underwent echocardiography while conscious using a doppler ultrasound machine (Philips Inc., Bothell, WA, U.S.A.). An S12-4 scan probe was used to trace the short views of the quadrilocular structure by a professional echocardiographer. Concrete parameters were measured for at least three consecutive cardiac beats as follows: left atrial diameter (LAD), right atrial diameter (RAD), left ventricular end-diastolic dimension (LVEDd), left ventricular end-systolic dimension (LVESd), and left ventricular ejection fraction (LVEF) [13].

Langendorff perfusion for rabbit heart

The heparinized rabbits were killed and positioned on a specially designed experimental table. An inverted 'T' thoracotomy was applied to expose the whole heart. The heart was cut off along the dorsal lung using tweezers to hold the lung up and transferred into a glass with precooling KH fluids quickly (in mmol/L: NaCl, 119; KCl, 4; $CaCl_2$, 1.8; $MgCl_2$, 1; NaH_2PO_4, 1.2; $NaHCO_3$, 25, and glucose, 10). Redundant tissues around the aorta were removed, and the aorta was placed carefully over the perfusion needle and fixed by surgical sutures. The prepared KH fluids were gently pushed into the aorta to pump out the residual blood. Finally, the Langendorff apparatus was launched to perfuse the whole rabbit heart with the Tyrode's solution at 30 ml/min and the temperature of $37 \pm 0.5^{\circ}$C.

Optical mapping for *ex vivo* electrophysiology

After 15 min of stabilization, 128-channel electrodes were attached to four chambers (left atria, right atria, left ventricle, and right ventricle) of the hanging heart to record electrical signals in the normal rhythm condition. Then, the ECG electrodes were placed on the bilateral sides of the heart to document heart rate. Blebbistatin (MCE Inc., New Jersey, U.S.A.), an excitatory contraction uncoupling agent, was added to the perfusate to eliminate the artifacts during optical mapping. After adding the Pluronic F127 (a surfactant assisting larger water solubility of calcium-sensitive dye, CAS9003-11-6, Sigma-Aldrich) into perfusate for 10 min, calcium indicator RhoD-2 (Life Technologies, Carlsbad, CA, U.S.A.) was slowly injected into the perfusion tank and circulated for 15 min. Next, the voltage-sensitive dye RH237 (MCE Inc., New Jersey, U.S.A.) was slowly infused into the perfusion system, and the heart filled with dyes was moved into the imaging room. The left atrium was excited by a laser light at a wavelength of 530 ± 25 nm. Band-pass filtering was performed at 511–551 nm to capture the light signals (LEDC-2001, MappingLab, U.K.). As previously reported [28], the emission light from the left atrial was assembled to an objective, and the light signals were separated using a beam-splitting dichroic mirror at 630 nm. V_m signals, a long wavelength, were filtered at 700 nm, and cardiac Ca^{2+} signals, a short wavelength, were filtered at 590 nm. Two CMOS cameras (OMS-PCI-2002, MappingLab, U.K.) enabled to obtain fluorescence signals from the heart at a sampling rate of 0.9 kHz [29].

Raw data was disposed of using OMapScope5 software (MappingLab, U.K.). Original optical signals were optimized for further visualization in the following setting: Gauss Smooth Parameter (smooth: 9×9; Theta: 2), Detrend Parameter (Order: 3), Zero-phase Median Filter (Window: 35), and Highpass Filter Parameter (Freq-Cut: 2; Family: Butterworth; Order: 2). S1-S2 pattern was chosen to measure the ERP (8 programmed S1 stimuli with a premature S2 decreased in steps of 5 ms; S1S1 interval = 3 Hz), and the S1S1 pattern was taken to induce the APD or CaT alternans (burst pacing for 1 s; S1S1 interval = 50 Hz). The different repolarization extents of APD (APDx) and Ca^{2+} transient duration (CaDx) were calculated based on the sinus rhythm mode. The values of time to peak and AP morphology in different spatial regions were obtained from two-channels. Based on the S1-S2 pattern, the AERP of AP phase and RyR2 refractoriness of the CaT phase were determined by S2 stimuli ranging from 150 to 80 ms. Conduction velocity and conduction dispersion were also identified from the eight continuous S1S1 stimuli at the frequency of 3Hz. Based on the S1-S1 mode, AF inducibility was measured, and the spatially discordant alternans (SDA) of both V_m and Ca^{2+} signals were acquired. The calculation and biological explanation of these measurement indicators in our study conformed to the prior criterion [30].

Phospho-proteomics

Precooling tissue samples were ground, lysed, and quantified using a BCA kit (PC0020, Solarbio, China). Further enzymolysis was conducted with the pancreatic ferment overnight at 37°C (1:50 mass ratio). All peptide fragments were labeled according to the tandem mass tag (TMT) kit and segmented using the C18 TIP column. All segmentations were dissolved in enrichment buffer fluid, and the liquid supernatants were transferred to the IMAC material for the modificatory enrichment. Mass spectrometry (MS) analysis was started after a separation process with EASY-nLC 1000 ultra-high performance liquid phase system. Secondary MS data were searched using

Maxquant (v1.5.2.8), and the bioinformatics analysis was carried out after a standard quality control step. The analyzed tools were as follows: data resolution (Maxquant, v.1.5.2.8 http://www.maxquant.org/), Go annotation (InterProScan, v.5.14-53.0 http://www.ebi.ac.uk/interpro/), and Heatmap clustering (R Package heatmap, v.2.0.3 https://cran.r-project.org/web/packages/cluster/).

Histology study

Left atrial tissues were segmented into the small pieces. They were then embedded in paraffin after fixing in 4% paraformaldehyde for 24 h. Masson's trichrome staining was performed on 5 μm tissue slides. The collagen-positive area reflected the extent of cardiac fibrosis, which was quantified using seven independent bright field microscopic images at 20× enlargement per animal and analyzed by ImageJ software (version 1.8.0) [29].

ELISA assay

Plasma samples and tissue homogenate were prepared to detect β1-AAb titers and cAMP concentration using an ELISA kit (ml057902, Mlbio, China). Samples were diluted to 50 μl at a 1:1 ratio by specimen diluent and added to the reaction well. A 50 μl biotin-labeled primary antibodies were added to a 96-well plate after supplementing 50 μl standard with 50 μl sample liquids. The samples were incubated under 37°C for 1 h. After washing three times, 80 μl HRP-streptomycin was added to the well and incubated at 37°C for 0.5 h. The cleaning operation was repeated three times, as mentioned above. A 50 μl substrate A and 50 μl substrate B were respectively merged into wells for 10 min, and the total reaction was stopped by 50 μl terminates. OD value was measured at the wavelength of 450 nm.

Atrial fibroblast isolation and culture

The whole heart of the Sprague-Dawley rat at 10-week-old was exposed by thoracotomy. Double-sided atria were excised and placed in a sterile glass bottle. Atrial tissues were soaked in PBS solution, and then were minced into pieces (1 × 1 × 1 mm). A bottle was supplemented with 3 ml of a trypsin digestion solution containing 0.1% type II collagenase (Worthington, Biochemical, NJ, U.S.A.) for sufficient tissue digestion. The upper suspension was removed after 5 min. The complete Dulbecco's modified Eagle's medium (DMEM plus 10% fetal bovine serum, Gibco, Grand Island, NY, U.S.A.) was added to resuspend atrial tissue, and this flow was repeated seven times. The total cell suspension was filtered through a 200-mesh stainless steel screen and sub-packaged in 50 ml centrifuge tubes for centrifugation (800 rpm, 5 min). After removing the supernatants, cells were cultured in a 4 ml complete Dulbecco's modification of Eagle's medium Dulbecco (DMEM medium) at 37°C in an incubator with 5% CO_2. After 1 h, adhering cells were identified as the atrial fibroblast by the principle of differential velocity adherent. Fibroblasts were passaged 1: 2, and the second generation was chosen for subsequent study.

Exogenous β1-AAb intervention

HL-1 cell lines were transferred in 90 mm dishes (ZQ0920, Shanghai Zhong Qiao Xin Zhou Biotechnology Co., Ltd., China) and cultured with the complete medium (MEM medium, Gibco, C11095500BT; 10% fetal bovine serum, Gibco, 10099-141; 100 U/ml penicillin/streptomycin, Biological Industries, 04-001-1ACS) in cell incubator with 5% CO_2 and 95% air at 37°C. Monoclonal β1-AAbs (China Peptides) were kindly gifted by Prof. Huiyu Zhao from Capital Medical University [31]. Hybridoma was performed by the fusion of splenocytes from *BALB/c* mice with SP2/0 myeloma cell line. Monoclonal β1-AAbs were produced by the hybridoma clones and chosen for the subsequent *in vitro* experiment. The concentration of autoantibodies stimulation was determined by the CCK-8 assay (Supplementary Figure S1A,B). The second-generation HL-1 cells and fibroblasts were seeded into 6-well plates with PBS (vehicle group), 1 μmol/L β1-AAb (β1-AAb group) and 1 μmol/L β1-AAb + 1 μmol/L bisoprolol (bisoprolol group) for 48 h. Bisoprolol was preconditioned 1 h ahead before the β1-AAb administration.

Western blotting

Homogenates were prepared from the left atrial or cell samples and lysed using mixed cell lysates (RIPA: PMSF: phosphatase inhibitor cocktail = 100: 1: 1, Solarbio, China). Protein concentration was measured using a BCA assay kit (PC0020, Solarbio, China). Mini-PROTEAN Tetra (Bio-rad) electrophoresis was performed with 20 μg of protein loaded onto a 10% SDS-PAGE gel (80 V, 140 min). Proteins were transferred on PVDF membranes by wet transfer (300 mA, 90 min). The blocking process was performed in 5% BSA blocking solution at room temperature for 1 h, while the PVDF membranes were incubated with the primary antibodies overnight at 4°C. The following primary antibodies were utilized: anti-CaMKII (PA5-22168, Thermo Fisher, U.S.A.); anti-phospho-CaMKII (LS-C354565, Lifespan, U.S.A.); anti-RyR2 (MA3-916, Thermo Fisher, U.S.A.); anti-phospho-RyR2 (LS-C358303, Lifespan, U.S.A.);

Clinical Science (2023) **137** 195–217
https://doi.org/10.1042/CS20220654

anti-SERCA (MA3-910, Thermo Fisher, U.S.A.); anti-PLB (MA3-922, Thermo Fisher, U.S.A.); anti-phospho-PLB (ab15000-50, Abcam, U.S.A.); NCX (MA3-926, Thermo Fisher, U.S.A.); and GAPDH (ab125247, Abcam, USA).

Immunofluorescence

Atrial fibroblasts were plated on glass slides in 6-well plate for immunostaining. Adhering cells were fixed in 4% paraformaldehyde for 15 mins at the room temperature. About 100 μl mixed liquor (PBS: 0.5%Triton-100: 10% donkey serum = 200: 1: 10) was dropped on every slide to block and rupture membrane for 1 h. Cell slides were incubated overnight at 4°C with the primary antibodies (α-SMA, 1:500 dilution, Proteintech, U.S.A., No.14395-1-AP; CoL1, 1:500 dilution, Proteintech, U.S.A., No.66761-1-Ig). The primary antibodies were washed out using PBS for three times the next day. Then, slides were incubated in room temperature for 1 h with the fluorescently labeled second antibody (1:50 dilution, Proteintech, USA, No. SA00007-1). Slides were sealed and mounted by Dapi-Fluoromount-G (SouthernBiotech, China, No.0100-20). Images were photographed by a fluorescent microscope (OLYMPUS, U-TV0.63XC, Tokyo, Japan).

Statistical analysis

Original data were input into Excel version 2021 and were analyzed using SPSS version 26.0. Continuous variables were described as means ± standard deviations, and constituent ratio was represented as a percentage. Continuous variables were compared among the three groups using univariate ANOVA with Bonferroni (homogeneous variance homogeneity) or Games-Howell correction (heterogeneous variance homogeneity) for post-hoc comparisons. The constituent ratio of the three groups was analyzed using Pearson's chi-square. Repeated measurement data were measured using One-way Repeated Measures ANOVA with Bonferroni post-hoc comparison. If Mauchly's test of sphericity is not robust, when epsilon (ε) < 0.75, the Greenhouse-Geisser method was selected for correction. Pearson correlation was utilized for the correlation between two normally distributed quantitative variables. A two-tailed P-value < 0.05 was determined as the statistical significance. All statistical graphics were exported from GraphPad Prism 9 and the optical curve images were exported from Origin Pro 2018.

Results

The β1-AAb decreases the atrial electrical instability and increases the AF susceptibility

The systemic β1-AAb titers and atrial cAMP contents revealed a successful active immunization model. After the first β1AR-ECL2 inoculation, β1-AAb concentrations remained elevated in the immune and treatment groups compared with control group from the second week to the eighth week ($P<0.05$, Figure 1D). Meanwhile, the higher cAMP levels of the immune and bisoprolol group supported a positive β1AR-activited effect induced by β1-AAb ($P<0.05$, Figure 1E). Before the electrophysiological study, noninvasive ECG monitoring showed a significantly increased heart rate and P wave dispersion in the β1-AAb group in comparison with the control or bisoprolol group ($P<0.05$, Figures 1B,C). Endocardial electrophysiological parameters were measured to evaluate the atrial electrical stability under the β1-AAb stimulation. As reported in our prior work [13], β1-AAb shortened the AERP and stretched the WOV in the rabbits responding to active immunization, which were reversed by blocking β1AR (respectively, $P<0.05$, Figure 2D,E and Supplementary Figure S2). AF inducibility was significantly elevated in the β1-AAb group under the burst pacing, as well as the AF duration. However, bisoprolol exerted an anti-arrhythmic function by reducing AF susceptibility ($P<0.05$, Figure 2A–C,F,G).

The β1-AAb promotes the atrial enlargements and atrial fibrosis

Figure 3A depicts the typical echocardiographic images of the three groups. Rabbits with β1AR-ECL2 presented the prominent atrial enlargement characterized by increased LAD and RAD. Compared with the atrial sizes of the β1-AAb group, bisoprolol partly prevented the atrial structural remodeling, especially for right atrium ($P<0.05$, Figure 3B,C). Moreover, β1-AAb harmed cardiac function and promoted the ventricular structure alterations, including dilated LVEDd, LVEDs, and reduced LVEF ($P<0.05$, Figure 3D–F). Pearson's linear analysis evinced a positive correlation of β1-AAb titers of the eighth week with LAD and RAD (LAD: $r=0.475$; RAD: $r=0.709$, respectively, $P<0.05$, Figure 3G,H). A histology study revealed pathological changes underlying the atrial remodeling. Masson's trichrome staining displayed the extensive extracellular matrix accumulation and collagen deposition of left atrium in β1-AAb groups, while these decreased in bisoprolol group ($P<0.05$, Figure 3I,J). Meanwhile, total collagen areas displayed a positive correlation with β1-AAb titers of the eighth week ($r=0.592$, $P<0.05$, Figure 3K). The evidence

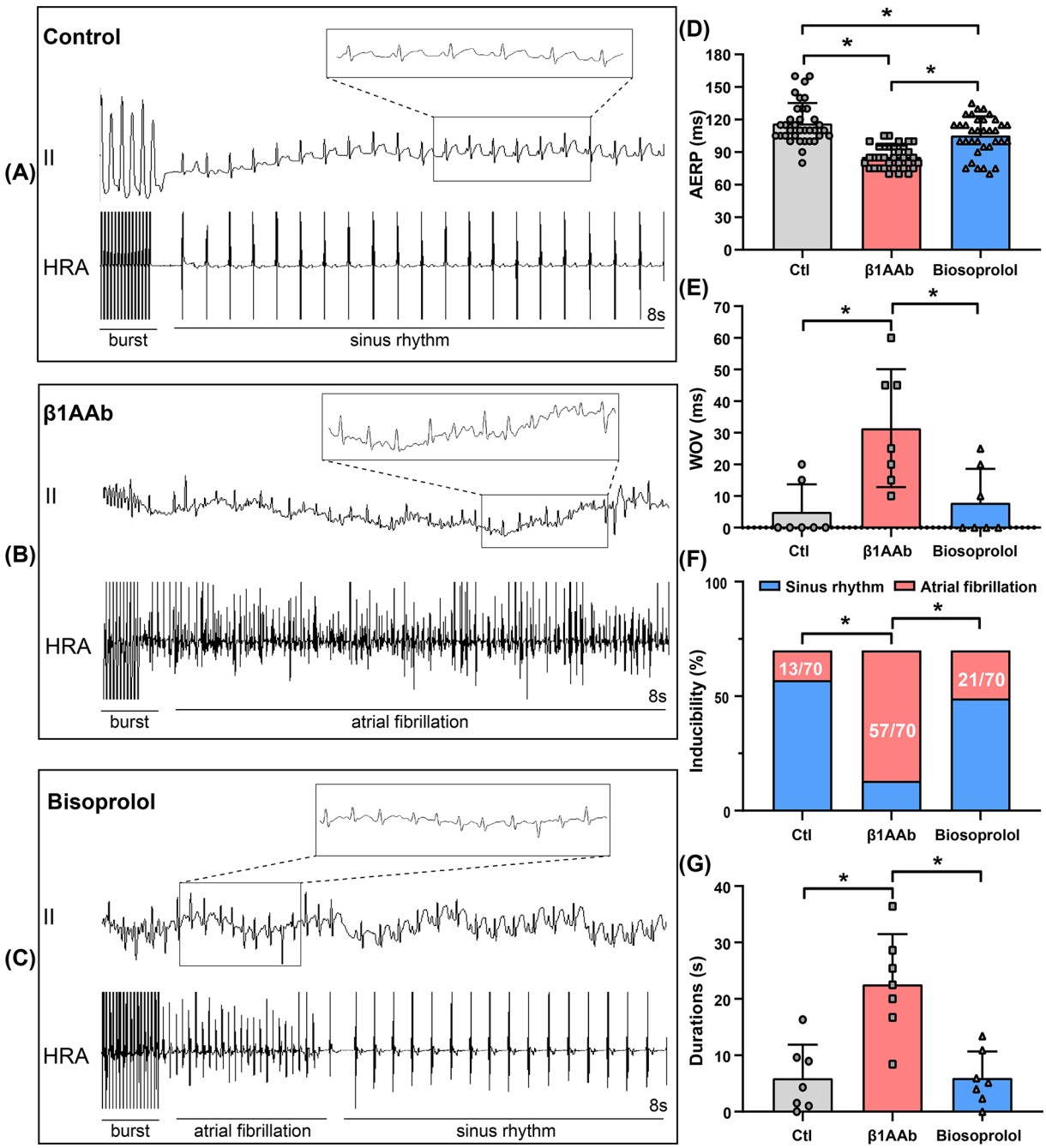

Figure 2. The β1-AAb decreases the atrial electrical instability and increases the AF Susceptibility

(**A–C**) typical images of AF induction with burst pacing at 50 ms S1-S1 interval among three groups. (**D**) repeating AERP measurements per animal for 5 times of three groups, (n=7) per group. (**E**) Calculation of atrial WOV during the electrophysiology study, (n=7) per group. (**F**) Repeating AF inducibility per animal 10 times of three groups, (n=7) per group. (**G**) Accumulated durations of AF episodes during AF induction, (n=7) per group. *P<0.05 indicates statistical significance.

above portended an ameliorative effect of weakening β1-AAb on cardiac dysfunction, atrial expansion, and atrial fibrosis.

The β1-AAb involves in the APD alterations via *ex vivo* optical mapping

In the V_m phase, four sites were chosen to record the repolarization of AP to a different extent (Figure 4A). Figure 4C

Clinical Science (2023) **137** 195–217
https://doi.org/10.1042/CS20220654

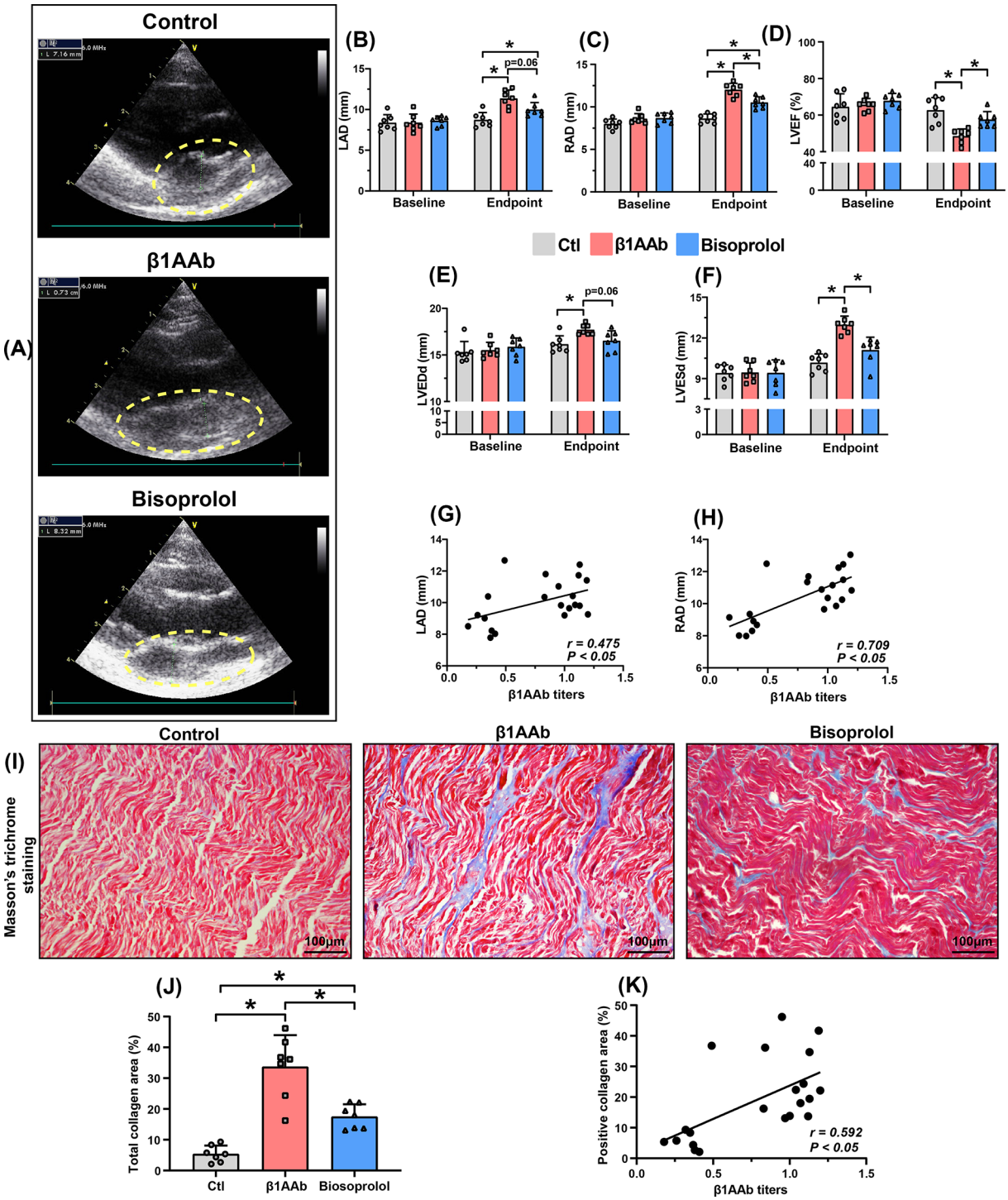

Figure 3. The β1-AAb promotes the atrial enlargements and atrial fibrosis

(**A**) Schematic diagram of echocardiography of three groups. Yellow circle indicates LA location. (**B–F**) comparison of LAD, RAD, LVEF, LVEDd, and LVESd among three groups at the baseline and endpoint, (n=7) per group. (**G,H**) Pearson correlation of the β1-AAb titers at the 8th week with atrial diameters, (n=7) per group. (**I**) Typical Masson's trichrome staining of left atrium among the three groups. The blue areas indicate the collagen depositions, (×20). (**J**) quantitative statistics of positive collagen areas, (n=7) per group, *P<0.05 indicates statistical significance. (**K**) Pearson correlation of β1-AAb titers at the 8th week with the positive collagen areas of atrium sections, (n=7) per group, *P<0.05 indicates statistical significance. *P<0.05 indicates statistical significance. LAD, left atrial diameter; LVEDd, left ventricular end-diastolic dimension; LVEF, left ventricular ejection fraction; LVESd, left ventricular end-systolic dimension; RAD, right atrial diameter. *P<0.05 indicates statistical significance.

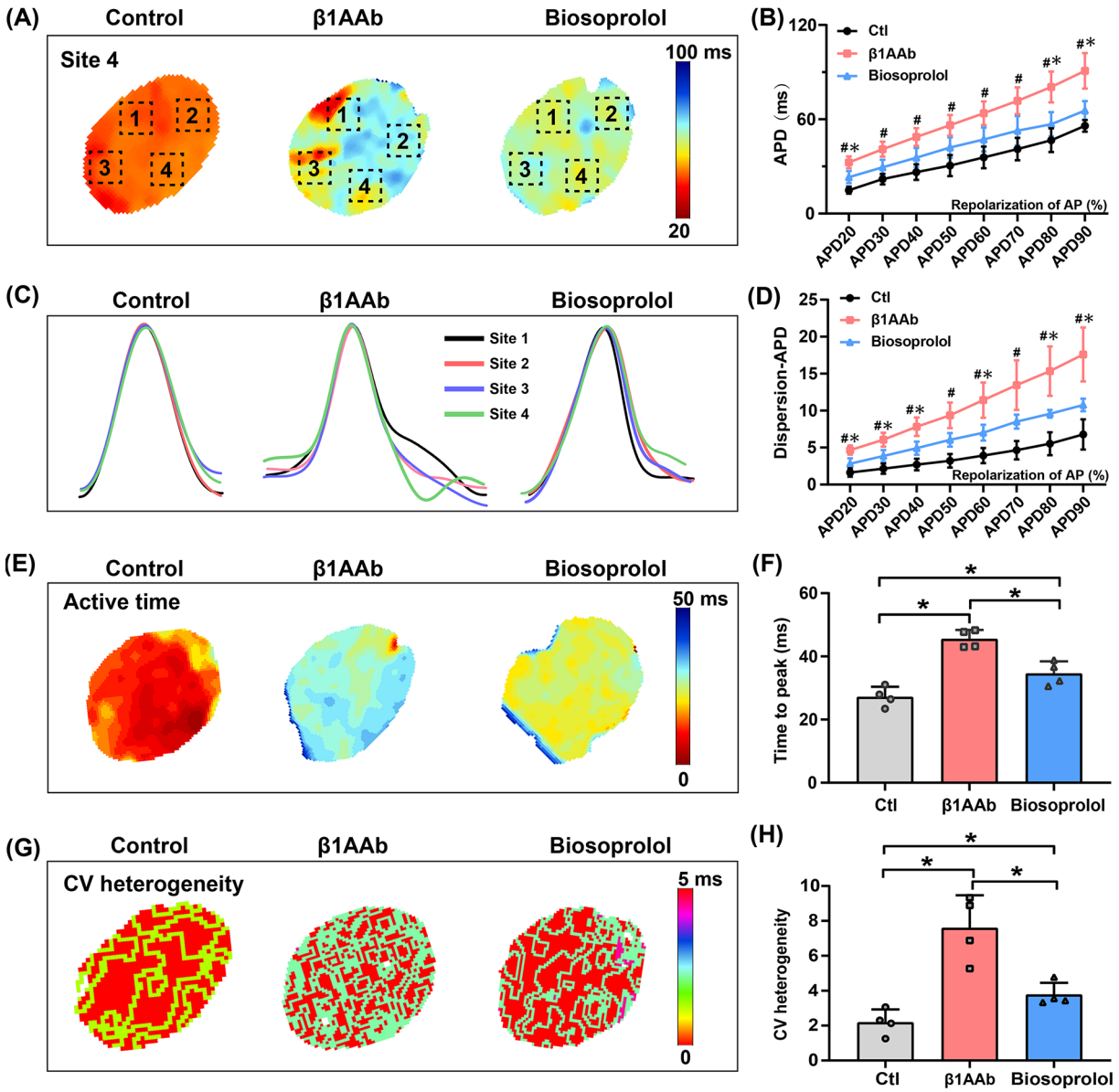

Figure 4. The β1-AAb involves in the APD alterations via *ex vivo* optical mapping

(**A**) Maps of APD80 with four recording sites of three groups under sinus rhythm. (**B**) Quantitative calculation from APD90 to APD20 of three groups, (n=4) per group. (**C**) APD80 tracks of four recording sites per isolated heart in three groups at the sinus condition. (**D**) Figuring of APD spatial variation per atrium from APD90 to APD20 of three groups, (n=4) per group. (**E**) Maps of active time mode per heart in three groups under sinus state. (**F**) Calculation of time to peak in AP phase each left atrium of three groups, (n=4) per group. (**G**) Heterogeneity of CV mapping of three groups under sinus heart rate. (**H**) Absolute value calculation of CV heterogeneity in three groups, (n=4) per group. *P<0.05 indicates statistical significance.

depicts the atrial AP morphology of four sites. APD prolongation of the β1-AAb group started from 20% repolarization compared with the control group, while repolarizations of APD80 and APD90 showed a meaningful reduction in bisoprolol group compared to β1-AAb group (P<0.05, Figure 4B). APD dispersion among four different sites was calculated by subtracting the minimum value from the maximum value. The coefficient of variation (COV) was equaled the standard deviation divided by mean. The β1-AAb increased spatial discrepancy and the COV of APD compared with other groups (P<0.05, Figure 4D and Supplementary Figure S3A). The β1-AAb had a remarkable delay in the time to peak and a larger conduction heterogeneity under sinus rhythm conditions, normalized by bisoprolol in some measure compared with control group (P<0.05, Figure 4E-H).

Clinical Science (2023) **137** 195–217
https://doi.org/10.1042/CS20220654

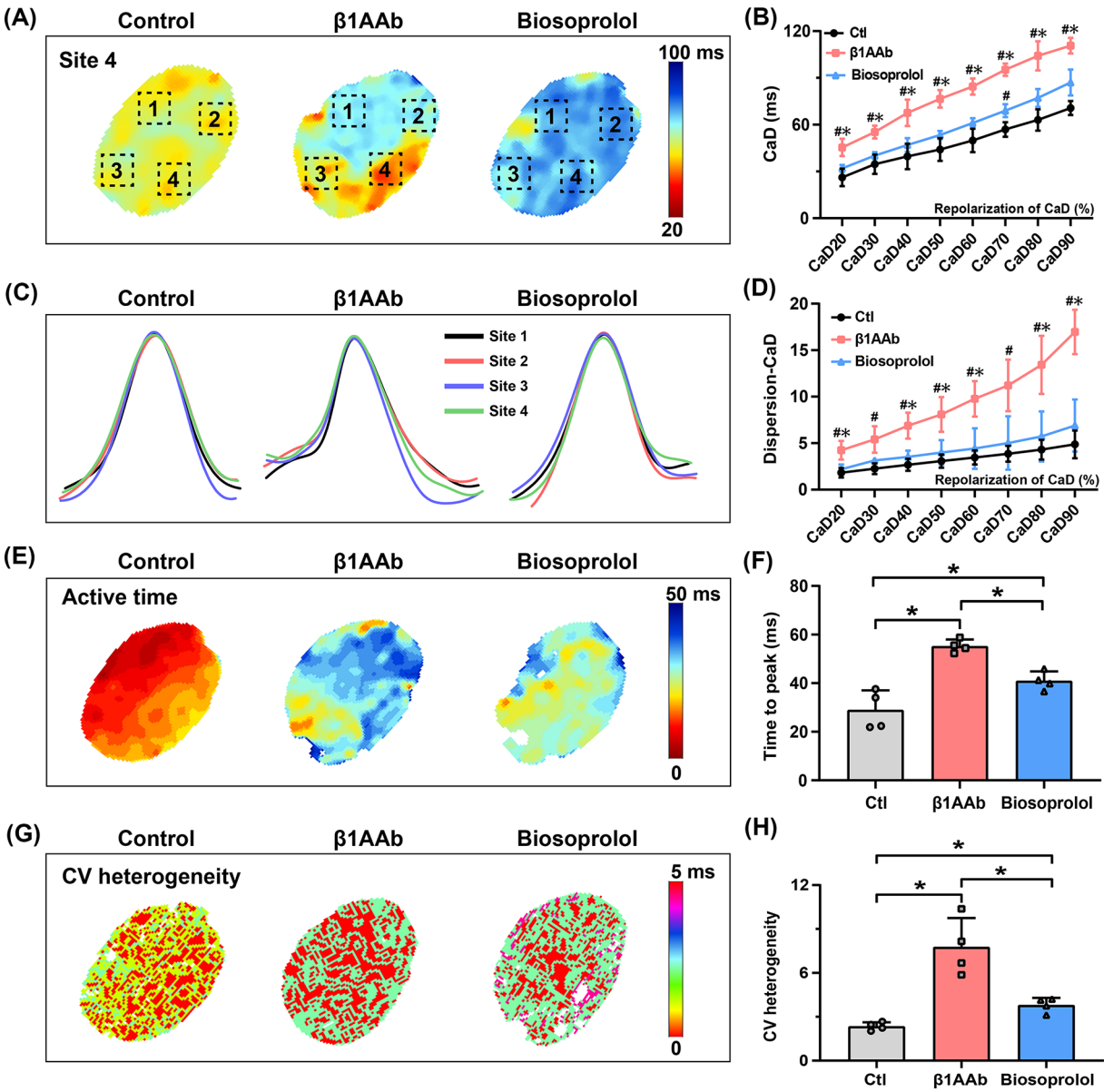

Figure 5. The β1-AAb facilitates CaD alterations at the isolated-heart level

(**A**) CaD80 maps with four recording sites of three groups under sinus rhythm. (**B**) Difference quantitation from CaD90 to CaD20 of three groups, (n=4) per group, $^{\#}P<0.05$ vs. control group; $^{*}P<0.05$ vs. bisoprolol group. (**C**) Delineation of CaD graph at four tracing sites among three groups in the condition of sinus rate. (**D**) Plotting of CaD dispersion of three groups, (n=4) per group. (**E**) Active time of Ca^{2+} signal channel among three groups in sinus state. (**F**) Quantitation of time to peak in CaD phase, (n=4) per group. $^{\#}P<0.05$ vs. control group; $^{*}P<0.05$ vs. bisoprolol group. (**G**) Heterogeneity of calcium wave dissemination per isolated heart of three groups based on sinus rhythm. (**H**) Calculation of Ca^{2+} wave propagation variation among three groups, (n=4) per group. $^{*}P<0.05$ indicates statistical significance.

The β1-AAb facilitates the CaD alterations at the whole isolated-heart level

Paralleled to the V_m phase, the Ca^{2+} phase unfolded a dynamic intracellular calcium flux under the background of sinus rhythm. Figure 5A shows four CaD map sites. Figure 5C exhibits that Ca^{2+} transients are manipulated by intracellular calcium signals and Ca^{2+} transients trace from different sites per group under normal conditions. Various

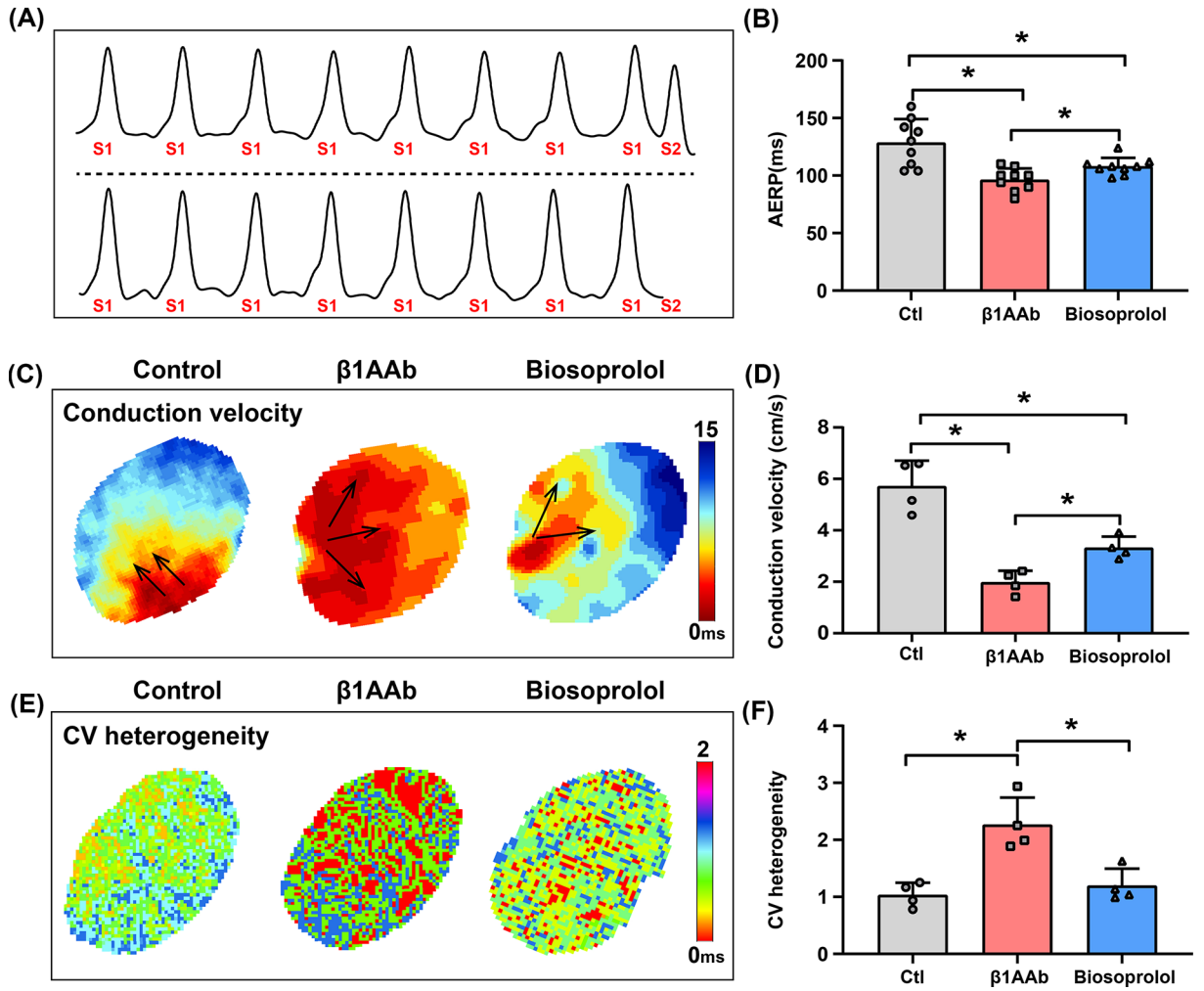

Figure 6. The β1-AAb impedes the atrial conduction properties

(**A**) Typical sketch map of pacing in a S1-S2 mode at 3 Hz. (**B**) Measurements of AERP at the *ex vivo* level per left atrium for at least two times among three groups, (*n*=4) per group. (**C**) Pacing-induced CV recording of three groups. (**D**) Calculation of CV under pacing at 3 Hz, (*n*=4) per group. (**E**) Synchronous detection of CV heterogeneity in three groups. (**F**) Quantitation of CV heterogeneity using S1-S2 protocol, (*n*=4) per group. *$P<0.05$ indicates statistical significance.

repolarization stages of CaD revealed the spending time on the different periods of intrinsic Ca^{2+} dynamic containing priming, eruption, and recession. The β1-AAb facilitated the CaD protraction from CaD20 to CaD90, while there were no significant differences of CaDs between the control and therapeutic groups except the CaD70 ($P<0.05$, Figure 5A,B). Moreover, bisoprolol effectively alleviated the spatial discrepancy, and the COV of CaD elicited by β1-AAb ($P<0.05$, Figure 5C,D and Supplementary Figure S3B). As for active time to peak and CV heterogeneity in the Ca^{2+} phase, bisoprolol effectively shortened the delayed active time and attenuated CV heterogeneity values when compared to the β1-AAb group ($P<0.05$, Figure 5E–H).

The β1-AAb impedes the atrial conduction properties

AERP measurement of the ex vivo optical mapping was performed with S1-S2 mode. AERP was decreased in the β1-AAb group but partly rescued by bisoprolol treatment ($P<0.05$, Figure 6A,B), resembling the endocardial electrophysiology results. Besides, atrial conduction velocity was measured simultaneously during eight consecutive S1 stimuli. Figure 6C shows that the β1-AAb altered the CV, aggravated multidirectional conduction and ectopic activity compared with the control group. Figure 6D displays quantitative results demonstrating that bisoprolol effectively recovered the CV compared with this index in the β1-AAb group ($P<0.05$). The CV heterogeneity of the rabbits with β1-AAb intervention was larger than in other groups ($P<0.05$, Figure 6E,F).

Clinical Science (2023) **137** 195–217
https://doi.org/10.1042/CS20220654

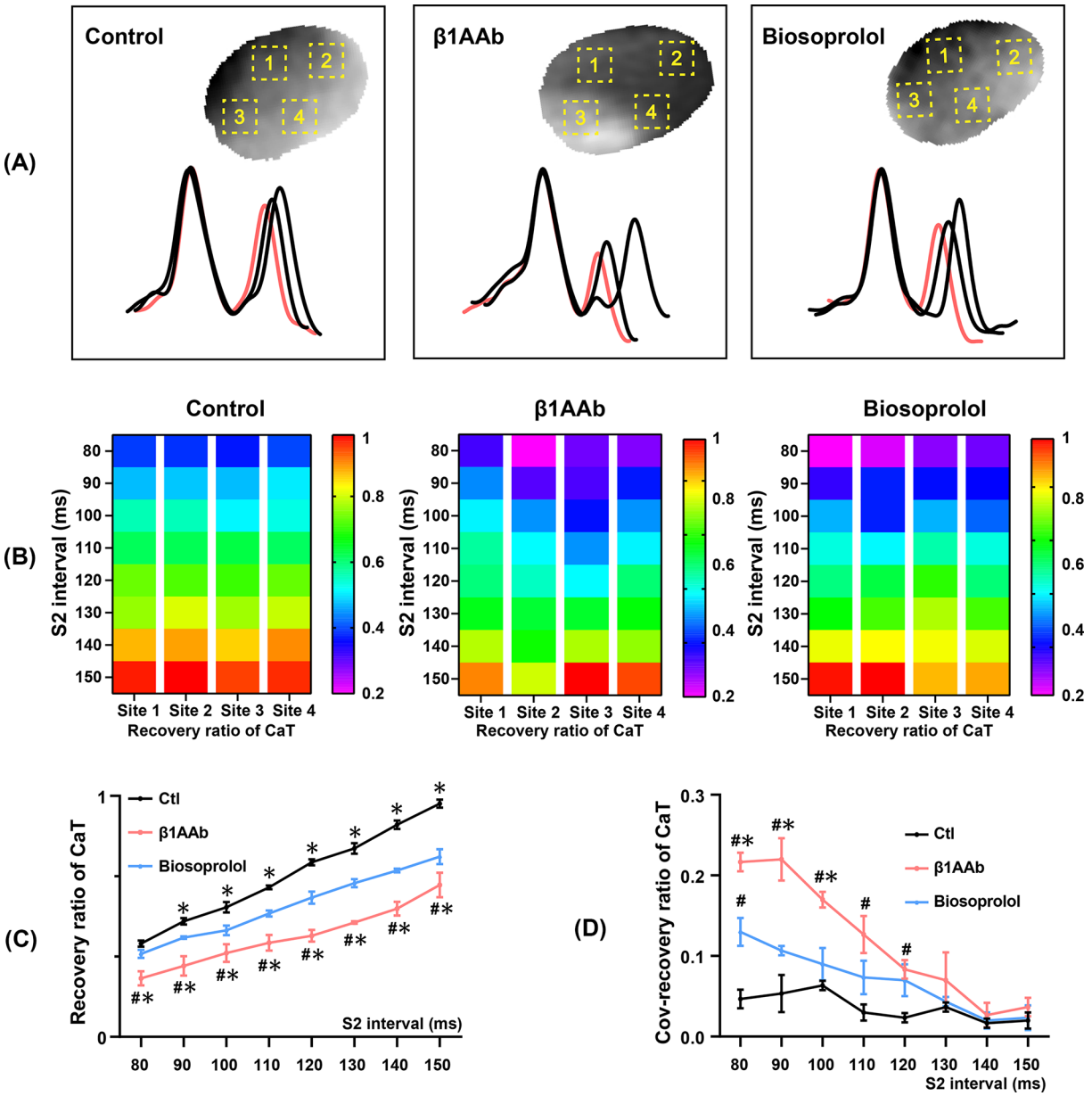

Figure 7. The β1-AAb prolongs Ca^{2+} transient refractoriness

(**A**) Overlapped CaT traces of four recording locations among three groups. (**B**) For four sites, intuitionistic heat maps of the recovery ratio of CaT with the decreased S2 intervals in three groups. (**C**) Depiction of recovery ratio of CaT at the integral level, (n=4) per group, $^{\#}P<0.05$ vs. control group; $^{*}P<0.05$ vs. bisoprolol group. (**D**) Plotting of COV-recovery ratio of CaT, (n=4) per group, $^{\#}P<0.05$ vs. control group; $^{*}P<0.05$ vs. bisoprolol group.

The β1-AAb prolongs Ca^{2+} transient refractoriness

An S1 stimulus on cardiomyocytes evoked an intracellular Ca^{2+} release event. An extra S2 stimulus can arouse the next Ca^{2+} transient to a considerable amplitude in a normal state. When an S1 impulse induced an intracellular Ca^{2+} transient, the ratio of S2-induced CaT versus the preceding S1-induced CaT was determined as CaT refractoriness, also named RyR2 refractoriness. Figure 7A depicts the CaT trace following S1 stimulation combined with the final S2 stimulus. Heat maps showed the spatial heterogeneity of RyR2 refractoriness of four areas responding to the decremental S1-S2 intervals. A larger spatial heterogeneity of CaT recovery ratio was intuitively observed in the β1-AAb group than in other groups (Figure 7B). Figure 7C reveals the recovery of CaT at the whole atrium level. Bisoprolol

significantly increased CaT recovery with the different S2 intervals compared with the β1-AAb group quantifications but was unable to renovate them to the control group levels. The COV of CaT recovery ratio was described by standard deviation dividing mean [32]. In our study, the COV ratio of CaT in the β1-AAb group exceeded it in the control group or therapeutic group, indicating a prominent areal heterogeneity of Ca^{2+} release restitution capability ($P<0.05$, Figure 7D).

The β1-AAb augments the arrhythmogenic atrial alternans and re-entry

Atrial alternans were recorded using an S1-S1 protocol. We first tested the AF inducibility at the *ex vivo* dimension. Similar to *in vivo* results, AF inducibility and duration are increased in the β1-AAb group, but bisoprolol administration alleviated this effect ($P<0.05$, Figure 8A–C). Atrial APD alternans and CaT alternans ratio reflected repolarization dispersion and Ca^{2+} handling of per beat in an area. Spatial discordant pattern (SDA) manifested the repolarization dispersion among different areas. Figure 8D displays a typical SDA graphic. The SDA incidence was elevated in the β1-AAb group, and bisoprolol cure lowered it ($P<0.05$, Figure 8E). Furthermore, atrial alternans at the integral level were monitored synchronously. The β1-AAb exacerbated the APD alternans of a single site, increasing the arrhythmogenic CaT alternans ratio compared with the control and bisoprolol groups ($P<0.05$, Figure 9A–D). Figure 9E and 9F, respectively, show the direct tracings of consistent conduction and re-entry.

The potential mechanisms of atrial Ca^{2+} mishandling induced by β1-AAb

In the classical paradigm, signal transduction of the β1-AR signaling pathway was dependent on the substrate phosphorylation by upstream kinases [33]. The phospho-proteomic was performed to explore the significant biological direction underlying the active immunization models. In the β1-AAb group, 105 up-regulated proteins with 148 phosphorylation sites showed statistically significant differences in comparison with control samples. The volcano plot presents various modification sites on 14 molecules related to calcium handling and cAMP activation (Figure 10B). Especially in Figure 10A, five phosphor-sites on RyR2 significantly differ between the β1-AAb and control group, potentially pointing to the molecular origination of Ca^{2+} mishandling. Then, we tested the protein expressions of molecules related to calcium handling (Figure 10C). The β1-AAb effectively activated the CaMKII at the Thr286 site and its downstream RyR2 at the Ser2814 site, while these positive regulations showed the opposite tendency by blocking β1-AR ($P<0.05$, Figure 10D,E). ATPase sarcoplasmic reticulum Ca^{2+} transporting 2 (SERCA2α) and its repressor phospholamban (PLB) dominated the Ca^{2+} reuptake of SR. Bisoprolol partly reversed the down-regulation of SERCA2 and phosphorylated extent of PLB (Ser16) group compared with the β1-AAb group ($P<0.05$, Figure 10F,G). However, the protein expressions of sodium/calcium exchanger 1 (NCX) in the three groups were comparable ($P>0.05$, Figure 10H).

Exogenous β1-AAb intervention elicits cellular phenotypes to arrhythmia propensity of HL-1 cells and atrial fibroblasts

Exogenous β1-AAb intervention for 48 h induced a significant CaMKII and RyR2 activations of HL-1 cells, but blocking β1-AR prevented this positive regulation ($P<0.05$, Figure 11A–C). The expressions of SERCA2α were not significantly different among the three groups ($P>0.05$, Figure 11D). Figure 11E demonstrated that bisoprolol eradicated the passivation of PLB induced by the β1-AAb ($P<0.05$, Figure 11E). Besides, the β1-AAb promoted the phenotype transformation from atrial fibroblasts to myofibroblast by increasing alpha smooth muscle actin (α-SMA) and collagen 1 (Col 1) expressions, and bisoprolol eliminated this phenotype transformation to some extent ($P<0.05$, Figure 11F–I).

Discussion

This work mainly found as follows: (1) chronic β1-AAb stimulation reduces the atrial electrical stability including the shortened ERP, increased WOV and AF duration; (2) β1-AAb involves in the atrial structural remodeling and cardiac dysfunction featured by the atrial interstitial fibrosis; (3) β1-AAb alters the intrinsic APD and CaD properties and conduction performance; (4) β1-AAb exacerbates the calcium mishandling and augmented arrhythmogenic alternans and re-entry; (5) blocking β1-AR protects β1AAb-induced Ca^{2+} handling abnormality of atrial cardiomyocytes and suppresses myofibroblast phenotypes (Figure 12).

Our group seeks to imitate the hallmarks of AF subsets in autoimmune diseases by using an active immunization rabbit model as previously published [25]. Compared to the monoclonal β1-AAb [24], though the active immunization strategy is unable to investigate the dosage effect due to the lack of β1-AAb quantification, it is convenient to use autoimmune rabbit models to gain more electrophysiological parameters in vivo. Consistent with our previous

Clinical Science (2023) **137** 195–217
https://doi.org/10.1042/CS20220654

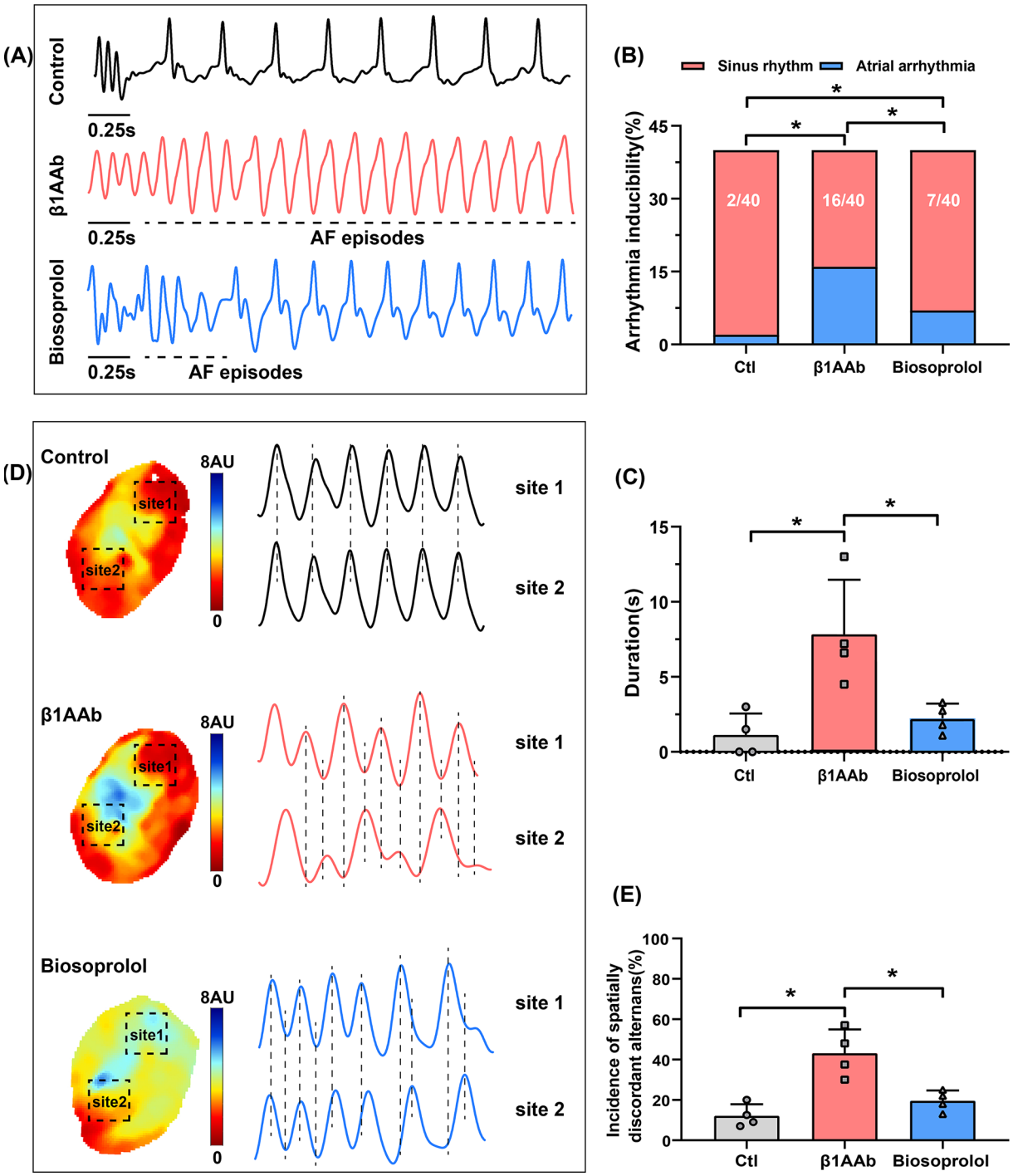

Figure 8. The β1-AAb potentiates the arrhythmogenic SDA

(**A**) Representative graphs of AF induction process. (**B**) Counting of the numbers of inducible AF per isolated heart among three groups, (n=4) per group. (**C**) Contrast in the duration of AF episodes in a S1-S1 protocol at 50 Hz, (n=4) per group. (**D**) Profiles of SDA phenomenon while tracing at two sites in three groups. (**E**) Calculation of the incidence of SDA, (n=4) per group. *P<0.05 indicates statistical significance; SDA, spatial discordant alternan.

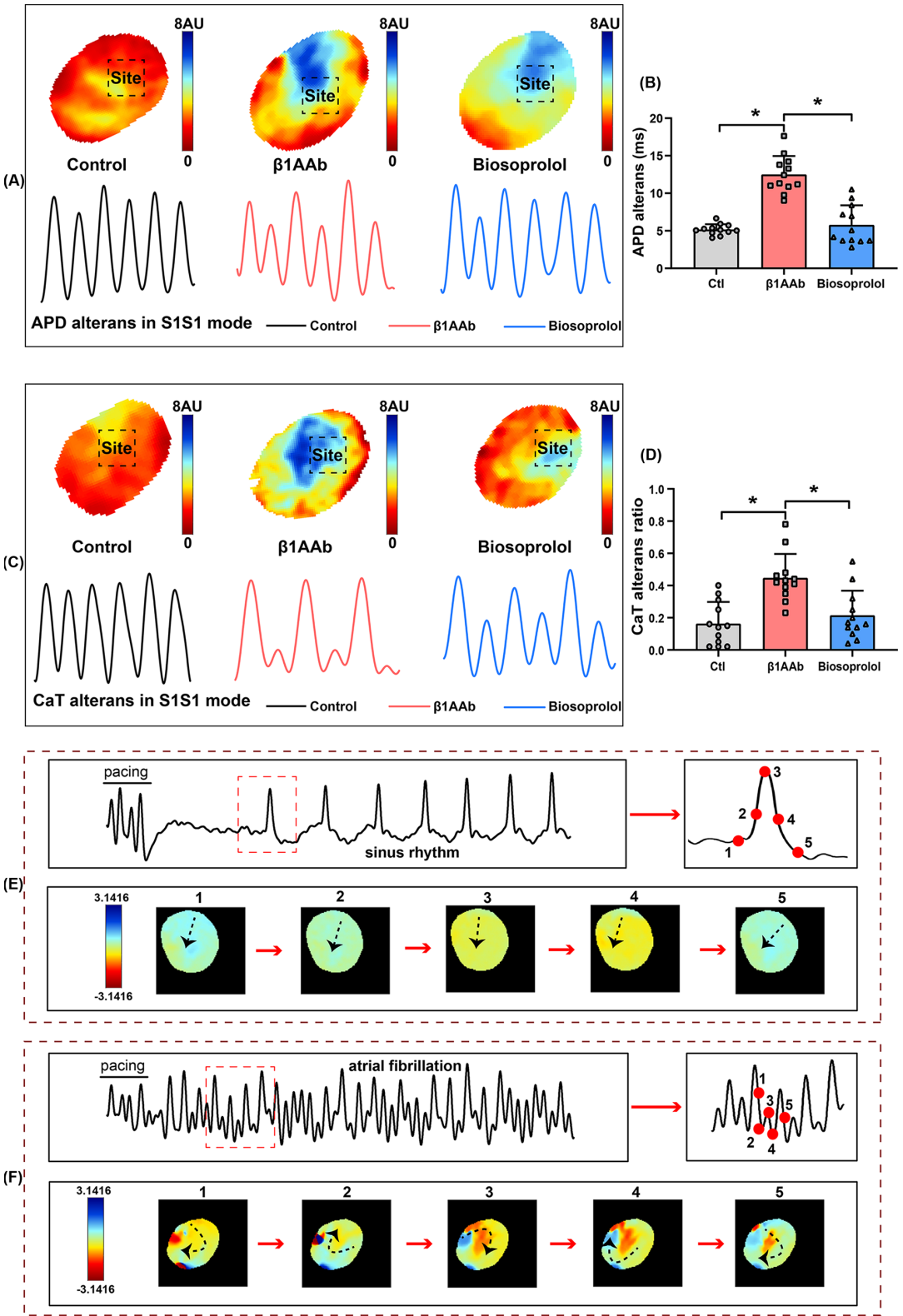

Figure 9. The β1-AAb augments the arrhythmogenic atrial alternans and re-entry

(**A**) Symbolic arrhythmogenic AP alternans at the whole-atrium dimension. (**B**) Quantitative statistics of APD alternans among three groups, (n=4) per group. (**C**) Representative images of CaT alternans under the burst pacing at 50 Hz. (**D**) Calculation of the CaT alternans ratio of three groups, (n=4) per group. *P<0.05 indicates statistical significance. (**E,F**) Re-entry recording in the process of AF induction at 50 Hz.

Clinical Science (2023) **137** 195–217
https://doi.org/10.1042/CS20220654

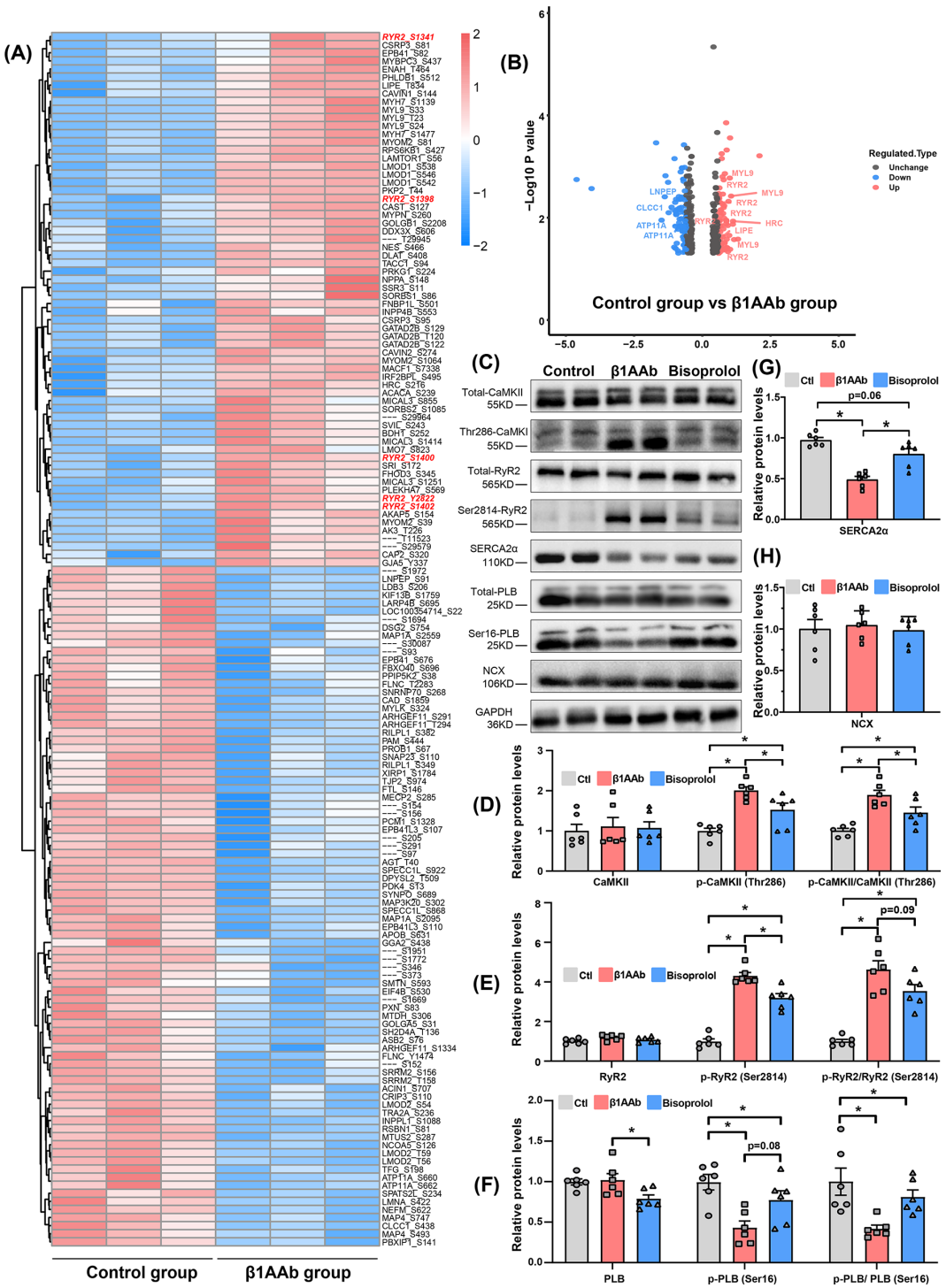

Figure 10. The potential mechanisms of atrial Ca^{2+} mishandling induced by β1-AAb

(**A**) Comparison of the differential phospho-sites on different genes between two groups from the mass spectrum results, (n=3) per group. (**B**) Volcano profile contains the differential phosphor-sites on genes related to intracellular calcium handling or cAMP signaling transduction. (**C–H**) Western blot results and quantitative statistics for CaMKII, p-CaMKII (Thr286), p-CaMKII/CaMKII, RyR2, p-RyR2 (Ser2814), p-RyR2/RyR2, PLB, p-PLB (Ser16), p-PLB/PLB, SERCA2α and NCX, (n=3) per group. *P<0.05 indicates statistical significance. CaMKII, calcium/calmodulin dependent protein kinase II; NCX, solute carrier family 8 member A1; p-CaMKII, phosphorylated calcium/calmodulin-dependent protein kinase II; PLB, phospholamban;p-PLB, phosphorylated phospholamban; p-RyR2, phosphorylated ryanodine receptor 2; RyR2, ryanodine receptor 2; SERCA2α, ATPase sarcoplasmic/endoplasmic reticulum Ca^{2+} transporting 2.

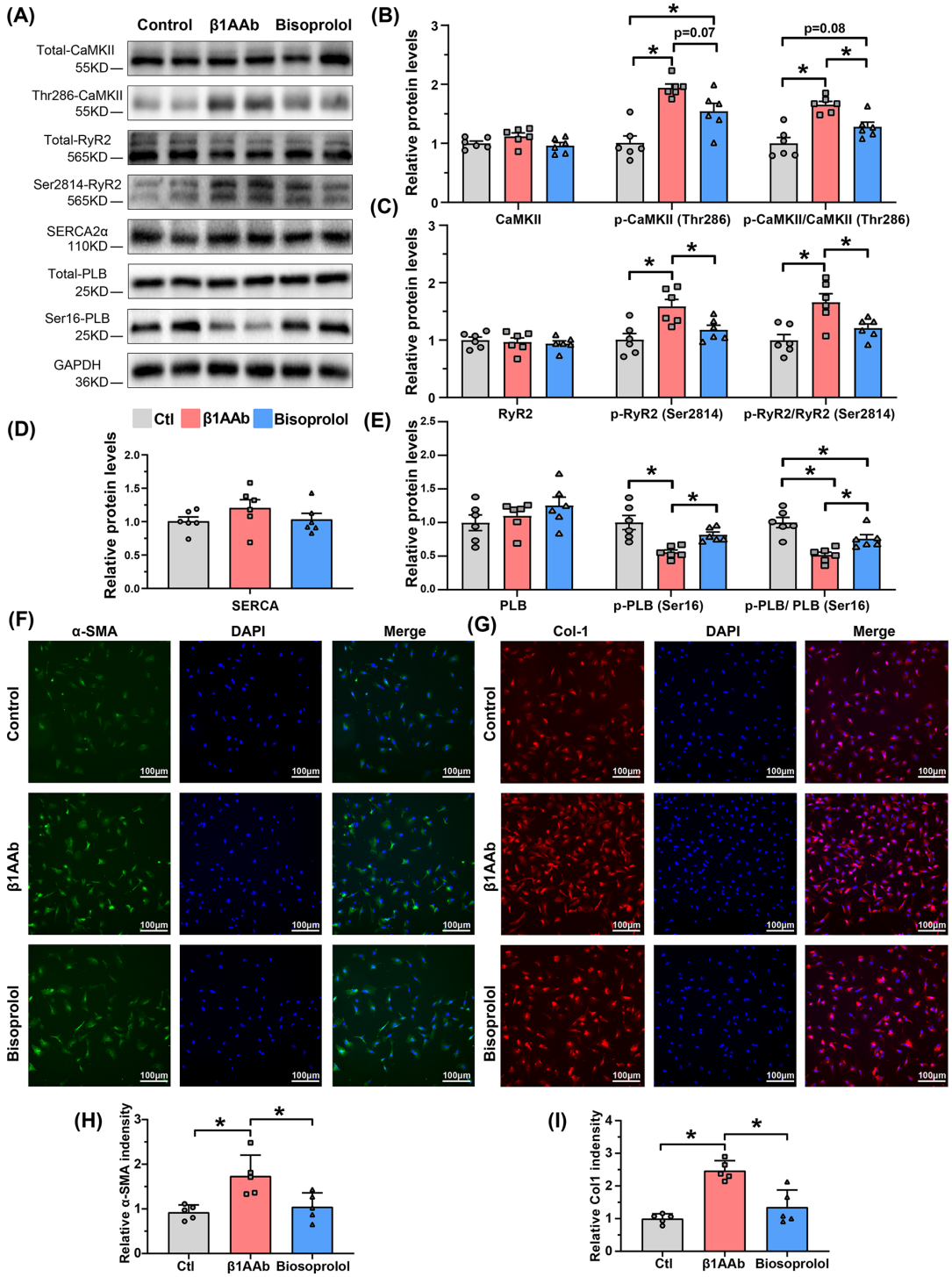

Figure 11. Exogenous β1-AAb intervention elicits cellular phenotypes to arrhythmia propensity of HL-1 cells and atrial fibroblasts

(**A–E**) Western blot results and quantitative statistics of HL-1 samples for CaMKII, p-CaMKII (Thr286), p-CaMKII/CaMKII, RyR2, p-RyR2 (Ser2814), p-RyR2/RyR2, PLB, p-PLB (Ser16), p-PLB/PLB and SERCA2α, (n=3) per group. (**F–I**) Immunofluorescence results on atrial fibroblasts with the α-SMA and collagen 1 and its quantitative statistics, (n=7) per group. *P<0.05 indicates statistical significance. α-SMA, α-smooth muscle actin; CaMKII, calcium/calmodulin dependent protein kinase II; p-CaMKII, phosphorylated calcium/calmodulin dependent protein kinase II; PLB, phospholamban; p-PLB, phosphorylated phospholamban; p-RyR2, phosphorylated ryanodine receptor 2; RyR2, ryanodine receptor 2; SERCA2α, ATPase sarcoplasmic/endoplasmic reticulum Ca^{2+} transporting 2.

Clinical Science (2023) **137** 195–217
https://doi.org/10.1042/CS20220654

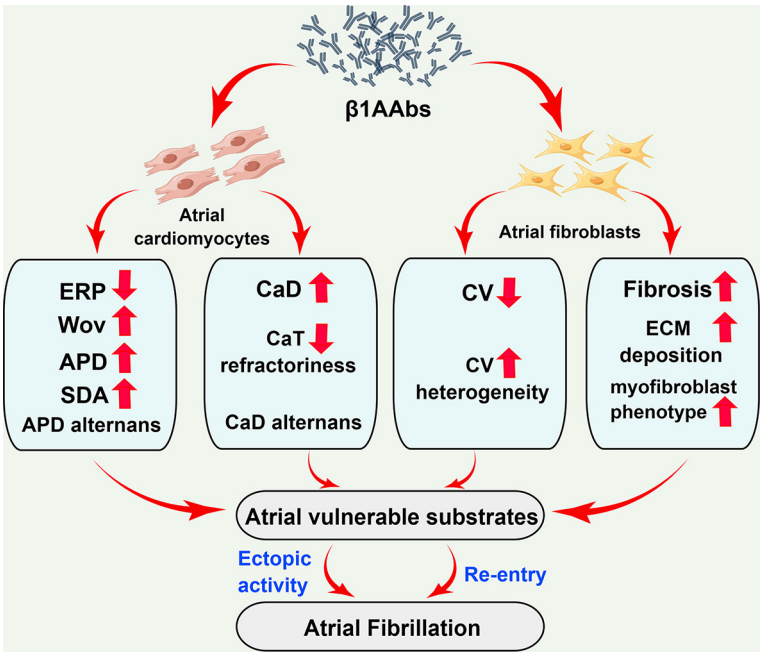

Figure 12. A schematic diagram of the potential mechanisms of the β1-AAbs in increasing AF vulnerability

The β1-AAbs contribute to the AF vulnerable substates via two pathways in the autoimmune models. The one is through mediating the calcium mishandling in atrial myocytes, the other is through promoting the atrial fibroblast phenotype to transform to the myofibroblast phenotype. These microscopic alterations create a susceptible circumstance for ectopic activities and re-entry.

results [13], systemic β1-AAb abundance keeps on the rise throughout the experiment, accompanied with the positive cardiac response. A successful autoimmune model in favor of performing the electrophysiology study. From a macroscopical view, electrophysiology and echocardiogram measurements indicate the contributions of β1-AAbs to canonical atrial electrical and structural remodeling. The curtate ERP and increscent WOV were observed in the experimental models, supporting an arrhythmogenic re-entry propensity that an ectopic activity falls into the vulnerable window [19]. Our previous work proved that the linear correlation between enlarged LAD and elevated β1-AAb titers was independent of clinical AF risk factors in paroxysmal AF patients [13]. In this study, a positive correlation of the β1-AAb concentrations with atrial size implies the specific effect of autoantibodies on the atrial structure. Furthermore, cardiac dysfunction modified by β1-AAb signifies an extensive harmful impact on holistic cardiomyocytes not merely in the bilateral atrium [24]. In the context of enlarged atrium sizes, the wide interstitial fibrosis phenotype occurring in left atrium will enable us to explain the structural changes challenged by β1-AAb from a pathological perspective.

To explore the exact atrial electrophysiological mechanisms underlying β1-AAb stimulation, our study carries out the optical mapping at the ex vivo level through V_m and Ca^{2+} signal channels. For the first time, we depict that bisoprolol partly reverses the increased APD and CaD, even the prolonged time to peak of left atrium after chronic β1-AAb stimulation based on sinus rhythm. Here, we can comprehend these results from the following two aspects. From the viewpoint of cellular electrophysiology, the duration of repolarization in the regional atrial myocardium coincides with the Ca^{2+} transient annihilation in the condition of sinus rhythm. From the angle of Ca^{2+} homeostasis, this altered repolarization velocity may functionally couple with intracellular Ca^{2+} mishandling in the absence of additional stimulus [30].

Under langendorff perfusion, we affirm the atrial ERP with a pre-set S1-S2 protocol. As expected, atrial ERP at the in vivo and ex vivo dimensions show a similar downward trend in the β1-AAb group. An interesting question issuing from our study is why the relationship between ERP and APD is not paralleled. In fact, these two are not conceptually unified as ERP emphasizes on the membrane depolarization capability, but APD mainly reflects the velocity of repolarization [34]. Prior works certainly demonstrated the vital actions of β1-AAb on lessening I_{k1}, I_{to} and prolonging APD in vitro [16]. Thus, a possible explanation for this question is that other ion transmembrane movements including I_{to} may implicate in this out-of-phase discrepancy [35]. Meanwhile, the reduced CV and disordered conduction

direction are magnified when pacing at a fixed frequency based on the cardiac fibrosis. Overall, ex vivo results further support that shortened ERP and slowed CV induced by β1-AAbs create a vulnerable substrate for re-entry at the integral-heart level.

To gain insight into Ca^{2+} handling disorder of β1-AAb-positive models underlying the changed electrophysiological properties, RyR2 refractoriness was evaluated using S1-S2 protocol. RyR2 refractoriness determines the cellular coordinate skills to pacing-induced calcium transients, so the greater the CaT recovery ratio, the greater the CaT amplitude elicited by S2 stimuli [36]. In our study, β1-AAb reduced the calcium transient refractoriness and enhanced the spatial dispersion of the CaT recovery ratio. From such results, we speculated that the smaller calcium transients pertaining to chronic β1-AAb interference may disable the Ca^{2+}-dependent inactivation of $I_{Ca(L)}$, upon restrict the Ca^{2+} efflux, produce the larger calcium storage in SR and lead to a longer CaD [36].

Burst pacing at 50 Hz was used to decipher more atrial vulnerable substrates to AF inducibility. Alternan, a repeated long-short-long-short pattern at higher rates was substantially comprehended as the repolarization dispersion. Discordant alternans of different regions were also described as SDA, presenting that the activities of atrial myocytes do not alternate in phases under burst pacing [37]. When this pattern of electrical signals is sometimes across atrial tissue, the wave-break occurs with a short refractory period in the center and long refractoriness in the neighbors [38]. Our work showed that AP alternans happen along with CaT alternans at times in autoimmune rabbits, insinuating β1-AAb mediates spatial inhomogeneous Ca^{2+} handling. Align with our results, Liu et al substantiated the crucial role of CaT SDA in causing AP SDA because they occur concurrently during burst induction [32]. Even though, the related synchronized mechanisms to AP and CaT SDA remain unclear.

To further make sense the potential molecular mechanism of abnormal Ca^{2+} handling, we selected key molecules according to the phospho-proteomics. The regulation of β1-AR signaling transduction depends on the phosphorylated modification initiated by a receptor ligand binding mode [25]. RyR2 expressed in the SR membrane modulates the cytosolic and SR Ca^{2+} concentrations [39]. RyR2 dysfunction favors diastolic calcium leak in a RyR2 remodeling-dependent manner, while phosphorylated RyR2 may be the driver of RyR2 leak [40]. In our study, five RyR2 phospho-sites were significantly upregulated in high throughput results. CaMKII, the upstream regulator of RyR2, which activates RyR2 at Ser2814 to increase the open probability and trigger Ca^{2+} sparks [41]. Our work displayed that β1-AAb effectively induces the CaMKII (Thr286) and RyR2 excitation (Ser2814), whereas blocking β1-AR with bisoprolol counteracts the phosphorylated modification. As mentioned before, intracellular Ca^{2+} mishandling may cause SR calcium overloading and lead to the subsequent RYR2 leak at the rapid rates. Meanwhile, the SR calcium contents are also perturbed by RyR2 leaky behavior in turn. More precisely, RyR2 leak not only causes the spontaneous ectopic activity like DADs but predisposes to the decreased thresholds of calcium wave formation and SR Ca^{2+} storage as well [20]. Thus, the abnormal atrial Ca^{2+} handling may achieve the functional unity with RyR2 derangement in arrhythmogenesis.

Besides, SERCA2α, which governs the SR calcium reuptake, was tested as another key regulator in this work. As its inhibitory protein, our results show that phospho-PLB up-regulates, whereas SERCA2α down-regulates in β1-AAb models, and bisoprolol can offer resilience to these alterations. Another question emerging from our study is what the potential role of down-regulated SERCA2α for Ca^{2+} handling in the context of β1-AAb administration. Lugenbiel et al certified that inactivated PLB, instead of protein expression itself, determines SERCA2α function [41]. Previous evidence from Briston et al notarized that increased SERCA2 function for Ca^{2+} buffering is to limit the arrhythmogenic calcium wave when applying β1-AR stimulation [42]. In contrast, Chen et al revealed that β1-AR activation mediates the SERCA2α stimulation will facilitate the refilling of SR and reinforce the SR loading [43]. As far as we concerned, the potentiated function of SERCA2α may be required for the SR calcium overloaded in β1-AAb group despite the down-regulated protein expression. However, the causative relationship between SERCA2α function and calcium kinetics still needs to be investigated.

In addition to the role of β1-AAb on atrial myocytes, we also explore β1-AAb modulation on fibroblasts as a supplement for our prior work [13]. Increased expressions of α-SMA on fibroblasts represent a distinct myofibroblast phenotype and secretion property. Collagen 1 is one of the secretory pro-fibrotic cytokines based on the myofibroblast phenotype, resulting in the deposition of interstitial collagen and local fibrosis [44]. Here, we discovered that β1-AAb promotes the fibroblasts phenotype transformation characterized by the higher expressions of α-SMA and Col 1, besides the effect on fibroblasts proliferation [45]. This micro-reaction may explain the contribution of β1-AAb on atrial conduction heterogeneity. In summary, β1-AAb blocking at the receptor level produces a beneficial effect on restoring the atrial remodeling in autoimmune AF subsets.

Clinical Science (2023) **137** 195–217
https://doi.org/10.1042/CS20220654

Limitations

The interpretations of our results should be cautious due to these several limitations. First, the solvent control cannot exclude the β1-AAb-mediated systemic immunological response to atriums. A better comparator may be an irrelevant peptide that will activate the rabbit immunization yet would not cause activation of β1-AR pathway. Second, signal smoothing and spatial integration of raw data limits the promotion of optical mapping results to real world. Third, the downstream events of Ca^{2+} mishandling containing DADs, Ca^{2+} sparks, and Ca^{2+} transients should be recorded utilizing Ca^{2+} image equipment or patch clamp in the following study. Fourth, our study is concentrated in describing the electrophysiological phenomenon in active immunization rabbits but is inattentive in delving into the molecular mechanisms of Ca^{2+} mishandling mediated by β1-AAb. Fifth, rescue manipulation by bisoprolol is only applied on β1-AR rather than on the downstream signal nodes of β1-AR. Sixth, this experimental design ignores the exact biological source of β1-AAb, and the abnormal immune system response related to β1-AAb production deserves exploration for future research.

Clinical implication

Early in 1998, elevated sera autoantibodies were identified among idiopathic paroxysmal atrial fibrillation [46]. To date, in the AF research field, sera β1-AAb levels have been successively reported regarding the reciprocal association with atrial fibrosis, the predictive value for AF recurrence post-ablation, and the detection of AF subsets with Graves' hyperthyroidism [47,12]. In AF field, the combinations of sera β1-AAb levels with the AF risk stratification or the AF prognosis estimation may be the promising research directions. It is well-known that β1-AR blocker for rate control is in a cornerstone position in AF management [48]. Our work found that bisoprolol against β1-AAb significantly ameliorates the atrial suspectable substrate and reduces AF inducibility. These preliminary results supported a potentially additional therapeutic effect of bisoprolol on the β1-AAb-positive AF subsets. Taken together, this work offers some new evidence from the autoimmune viewpoint in comprehending the intricate genesis of AF.

Conclusion

In conclusion, β1-AAb confers the atrial vulnerable substrates in autoimmune models via at least two different pathways. The one arrhythmogenic pathway is the induction of atrial Ca^{2+} mishandling through potentially mediating the CaMKII/RyR2 activation and RyR2-related SR calcium loading. Another pathway is involved in atrial fibrosis via potentially promoting the phenotype transformation from fibroblasts to myofibroblasts. β1-AR blocker significantly combats these two arrhythmogenic pathways.

Clinical perspectives

- Early in 1998, elevated sera autoantibodies were identified among idiopathic paroxysmal atrial fibrillation. To date, in the AF research field, sera β1-AAb levels have been successively reported regarding the reciprocal association with atrial fibrosis, the predictive value for AF recurrence post-ablation, and the detection of AF subsets with Graves' hyperthyroidism. In AF field, the combinations of sera β1-AAb levels with the AF risk stratification or the AF prognosis estimation may be the promising research directions.
- In AF field, the combinations of sera β1-AAb levels with the AF risk stratification or the AF prognosis estimation may be the promising research directions. It is well-known that β1-AR blocker for rate control is in a cornerstone position in AF management. Our work found that bisoprolol against β1-AAb significantly ameliorates the atrial suspectable substrate and reduces AF inducibility. These preliminary results supported a potentially additional therapeutic effect of bisoprolol on the β1-AAb-positive AF subsets.
- This work offers some new evidence from the autoimmune viewpoint in comprehending the intricate genesis of AF.

Data Availability

Datasets of this work are available from the corresponding authors as required.

Competing Interests

The authors declare that there are no competing interests associated with the manuscript.

Funding

This work is funded by the National Natural Science Foundation [grant numbers 81873488, 82260065, 82060069, 82100343, and 82160050] and the Natural Science Foundation of Xinjiang Uygur Autonomous Region [grant number 2021D01D16].

CRediT Author Contribution

Huaxin Sun: Conceptualization, Data curation, Validation, Writing—original draft. **Jie Song:** Data curation, Investigation, Writing—review & editing. **Kai Li:** Conceptualization, Data curation, Writing—review & editing. **Yao Li:** Data curation, Validation. **Luxiang Shang:** Conceptualization, Funding acquisition, Visualization. **Qina Zhou:** Data curation, Visualization. **Yanmei Lu:** Data curation, Software. **Yazhen Zong:** Data curation, Visualization, Methodology. **Xiuyuan He:** Supervision, Validation, Visualization. **Muzappar Kari:** Validation, Methodology. **Hang Yang:** Validation, Investigation, Visualization. **Xianhui Zhou:** Conceptualization, Funding acquisition, Visualization. **Ling Zhang:** Conceptualization, Funding acquisition, Writing—review & editing. **Baopeng Tang:** Conceptualization, Funding acquisition, Project administration, Writing—review & editing.

Ethics Statement

The *in vivo* experiments were authorized by the Animal Ethics Committee of the First Affiliated Hospital of Xinjiang Medical University (Approval number: IACUC-20170420-03). All studies conformed to the Basel Declaration and the principle of the Association for Assessment and Accreditation of Laboratory Care (AAALAC) [37].

Acknowledgements

We thank Dr. Yuhui-Zhao (Department of Physiology and Pathophysiology, School of Basic Medical Sciences, Capital Medical University, Beijing, China) for the gift of monoclonal β1-AAbs. We thank all colleagues of the animal center at Xinjiang medical university for animals feed and care. We thank Mei Ma, Yafan Han, Jiaru Cao and Wanyue Sang for the assistance in the invasive electrophysiologic study. We thank Scope research institute of electrophysiology for the platform supporting of optical mapping and data analysis. We thank PTM BIO biotechnology co., LTD for the phospho-proteomics service. We thank the Figdraw online tool from the platform of Home for Researchers (www.home-for-researchers.com).

Abbreviations

β1-AAb, β1-adrenergic receptor antibody; β1AR, β1 adrenergic receptor; AERP, atrial effective refractory period; AF, atrial fibrillation; APD, action potential duration; CaD, calcium transient duration; ECG, electrocardiogram; ECL, extracellular loop; LAD, left atrial diameter; RAD, right atrial diameter.

References

1 Kornej, J., Börschel, C.S., Benjamin, E.J. and Schnabel, R.B. (2020) Epidemiology of atrial fibrillation in the 21st century: novel methods and new insights. *Circ. Res.* **127**, https://doi.org/10.1161/CIRCRESAHA.120.316340
2 Nattel, S., Heijman, J., Zhou, L. and Dobrev, D. (2020) Molecular basis of atrial fibrillation pathophysiology and therapy: a translational perspective. *Circ. Res.* **127**, 51–72, https://doi.org/10.1161/CIRCRESAHA.120.316363
3 Gawalko, M., Balsam, P., Lodziński, P., Grabowski, M., Krzowski, B., Opolski, G. et al. (2020) Cardiac arrhythmias in autoimmune diseases. *Circ. J.* **84**, 685–694, https://doi.org/10.1253/circj.CJ-19-0705
4 Chen, S.K., Barbhaiya, M., Solomon, D.H., Guan, H., Yoshida, K., Feldman, C.H. et al. (2020) Atrial fibrillation/flutter hospitalizations among US medicaid recipients with and without systemic lupus erythematosus. *J. Rheumatol.* **47**, 1359–1365, https://doi.org/10.3899/jrheum.190502
5 Ellervik, C., Roselli, C., Christophersen, I.E., Alonso, A., Pietzner, M., Sitlani, C.M. et al. (2019) Assessment of the relationship between genetic determinants of thyroid function and atrial fibrillation: a mendelian randomization study. *JAMA Cardiol.* **4**, 144–152, https://doi.org/10.1001/jamacardio.2018.4635
6 Luo, Y., Liu, X., Ma, R., Wang, Y., Zimering, M. and Pan, Z. (2020) Circulating IgGs in Type 2 diabetes with atrial fibrillation induce ip-mediated calcium elevation in cardiomyocytes. *iScience* **23**, 101036, https://doi.org/10.1016/j.isci.2020.101036
7 Li, J. (2020) The Role of Autoantibodies in Arrhythmogenesis. *Curr. Cardiol. Rep.* **23**, 3, https://doi.org/10.1007/s11886-020-01430-x
8 Dragun, D., Philippe, A., Catar, R. and Hegner, B. (2009) Autoimmune mediated G-protein receptor activation in cardiovascular and renal pathologies. *Thromb. Haemost.* **101**, 643–648, https://doi.org/10.1160/TH08-10-0710
9 Nussinovitch, U. and Shoenfeld, Y. (2013) The clinical significance of anti-beta-1 adrenergic receptor autoantibodies in cardiac disease. *Clin. Rev. Allergy Immunol.* **44**, 75–83, https://doi.org/10.1007/s12016-010-8228-9

10 Chiale, P.A., Ferrari, I., Mahler, E., Vallazza, M.A., Elizari, M.V., Rosenbaum, M.B. et al. (2001) Differential profile and biochemical effects of antiautonomic membrane receptor antibodies in ventricular arrhythmias and sinus node dysfunction. *Circulation* **103**, 1765–1771, https://doi.org/10.1161/01.CIR.103.13.1765
11 Yalcin, M.U., Gurses, K.M., Kocyigit, D., Kesikli, S.A., Ates, A.H., Evranos, B. et al. (2015) Elevated M2-muscarinic and β1-adrenergic receptor autoantibody levels are associated with paroxysmal atrial fibrillation. *Clin Res Cardiol* **104**, 226–233, https://doi.org/10.1007/s00392-014-0776-1
12 Yalcin, M.U., Gurses, K.M., Kocyigit, D., Kesikli, S.A., Dural, M., Evranos, B. et al. (2015) Cardiac autoantibody levels predict recurrence following cryoballoon-based pulmonary vein isolation in paroxysmal atrial fibrillation patients. *J. Cardiovasc. Electrophysiol.* **26**, 615–621, https://doi.org/10.1111/jce.12665
13 Shang, L., Zhang, L., Shao, M., Feng, M., Shi, J., Dong, Z. et al. (2020) Elevated β1-adrenergic receptor autoantibody levels increase atrial fibrillation susceptibility by promoting atrial fibrosis. *Front. in Physiol.* **11**, 76, https://doi.org/10.3389/fphys.2020.00076
14 Du, Y., Zhang, S., Yu, H., Wu, Y., Cao, N., Wang, W. et al. (2019) Autoantibodies against β-adrenoceptor exaggerated ventricular remodeling by inhibiting CTRP9 expression. *J. Am. Heart Assoc.* **8**, e010475, https://doi.org/10.1161/JAHA.118.010475
15 Wang, L., Hao, H., Wang, J., Wang, X., Zhang, S., Du, Y. et al. (2015) Decreased autophagy: a major factor for cardiomyocyte death induced by β1-adrenoceptor autoantibodies. *Cell Death Dis.* **6**, e1862, https://doi.org/10.1038/cddis.2015.237
16 Zuo, L., Du, Y., Ma, J., Wang, K., Zhao, Y., Bai, F. et al. (2015) Pro-arrhythmic action of autoantibodies against the second extracellular loop of β1-adrenoceptor and its underlying molecular mechanisms. *Int. J. Cardiol.* **198**, 251–258, https://doi.org/10.1016/j.ijcard.2015.06.144
17 Nerbonne, J.M. and Kass, R.S. (2005) Molecular physiology of cardiac repolarization. *Physiol. Rev.* **85**, 1205–1253, https://doi.org/10.1152/physrev.00002.2005
18 Clarke, J.D., Caldwell, J.L., Pearman, C.M., Eisner, D.A., Trafford, A.W. and Dibb, K.M. (2017) Increased Ca buffering underpins remodelling of Ca handling in old sheep atrial myocytes. *J. Physiol.* **595**, 6263–6279, https://doi.org/10.1113/JP274053
19 Wijesurendra, R.S. and Casadei, B. (2019) Mechanisms of atrial fibrillation. *Heart* **105**, 1860–1867, https://doi.org/10.1136/heartjnl-2018-314267
20 Venetucci, L.A., Trafford, A.W. and Eisner, D.A. (2007) Increasing ryanodine receptor open probability alone does not produce arrhythmogenic calcium waves: threshold sarcoplasmic reticulum calcium content is required. *Circ. Res.* **100**, 105–111, https://doi.org/10.1161/01.RES.0000252828.17939.00
21 Santiago, D.J., Ríos, E. and Shannon, T.R. (2013) Isoproterenol increases the fraction of spark-dependent RyR-mediated leak in ventricular myocytes. *Biophys. J.* **104**, 976–985, https://doi.org/10.1016/j.bpj.2013.01.026
22 Houser, S.R. (2014) Role of RyR2 phosphorylation in heart failure and arrhythmias: protein kinase A-mediated hyperphosphorylation of the ryanodine receptor at serine 2808 does not alter cardiac contractility or cause heart failure and arrhythmias. *Circ. Res.* **114**, 1320–1327, https://doi.org/10.1161/CIRCRESAHA.114.300569
23 Chen, H., Cao, N., Wang, L., Wu, Y., Wei, H., Li, Y. et al. (2021) Biased activation of β-AR/Gi/GRK2 signal pathway attenuated β-AR sustained activation induced by β-adrenergic receptor autoantibody. *Cell Death Discov* **7**, 340, https://doi.org/10.1038/s41420-021-00735-2
24 Cao, N., Chen, H., Bai, Y., Yang, X., Xu, W., Hao, W. et al. (2018) β2-adrenergic receptor autoantibodies alleviated myocardial damage induced by β1-adrenergic receptor autoantibodies in heart failure. *Cardiovasc. Res.* **114**, 1487–1498, https://doi.org/10.1093/cvr/cvy105
25 Li, H., Scherlag, B.J., Kem, D.C., Benbrook, A., Shen, X., Cunningham, M.W. et al. (2014) Inducible cardiac arrhythmias caused by enhanced β1-adrenergic autoantibody expression in the rabbit. *Am. J. Physiol. Heart Circ. Physiol.* **306**, H422–H428, https://doi.org/10.1152/ajpheart.00551.2013
26 Iwata, M., Yoshikawa, T., Baba, A., Anzai, T., Nakamura, I., Wainai, Y. et al. (2001) Autoimmunity against the second extracellular loop of beta(1)-adrenergic receptors induces beta-adrenergic receptor desensitization and myocardial hypertrophy in vivo. *Circ. Res.* **88**, 578–586, https://doi.org/10.1161/01.RES.88.6.578
27 Xiaokereti, J., Guo, Y.-K., Dong, Z.-Y., Ma, M., Lu, Y.-M., Li, Y.-D. et al. (2021) Enhanced atrial internal-external neural remodeling facilitates atrial fibrillation in the chronic obstructive sleep apnea model. *PloS ONE* **16**, e0247308, https://doi.org/10.1371/journal.pone.0247308
28 Liao, J., Wu, Q.-F., Qian, C., Zhao, N., Liu, X., Zhao, Z.-Y. et al. (2020) TRPV4 blockade suppresses atrial fibrillation in sterile pericarditis rats. *JCI Insight* **5**, e137528
29 Wang, L., Myles, R.C., De Jesus, N.M., Ohlendorf, A.K.P., Bers, D.M. and Ripplinger, C.M. (2014) Optical mapping of sarcoplasmic reticulum Ca2+ in the intact heart: ryanodine receptor refractoriness during alternans and fibrillation. *Circ. Res.* **114**, 1410–1421, https://doi.org/10.1161/CIRCRESAHA.114.302505
30 Liao, J., Zhang, S., Yang, S., Lu, Y., Lu, K., Wu, Y. et al. (2021) Interleukin-6-mediated-Ca handling abnormalities contributes to atrial fibrillation in sterile pericarditis rats. *Front. Immunol.* **12**, 758157, https://doi.org/10.3389/fimmu.2021.758157
31 Gong, Y., Xiong, H., Du, Y., Wu, Y., Zhang, S., Li, X. et al. (2016) Autoantibodies against β1-adrenoceptor induce blood glucose enhancement and insulin insufficient via T lymphocytes. *Immunol. Res.* **64**, 584–593, https://doi.org/10.1007/s12026-015-8757-7
32 Liu, T., Xiong, F., Qi, X.-Y., Xiao, J., Villeneuve, L., Abu-Taha, I. et al. (2020) Altered calcium handling produces reentry-promoting action potential alternans in atrial fibrillation-remodeled hearts. *JCI Insight* **5**, e133754, https://doi.org/10.1172/jci.insight.133754
33 Wang, J., Gareri, C. and Rockman, H.A. (2018) G-protein-coupled receptors in heart disease. *Circ. Res.* **123**, 716–735, https://doi.org/10.1161/CIRCRESAHA.118.311403
34 Lo, A.C.Y., Bai, J., Gladding, P.A., Fedorov, V.V. and Zhao, J. (2020) Afterdepolarizations and abnormal calcium handling in atrial myocytes with modulated SERCA uptake: a sensitivity analysis of calcium handling channels. *Philos. Trans. A Math Phys. Eng. Sci.* **378**, 20190557, https://doi.org/10.1098/rsta.2019.0557
35 Fowler, E.D., Wang, N., Hezzell, M.J., Chanoit, G., Hancox, J.C. and Cannell, M.B. (2022) Improved Ca release synchrony following selective modification of I and phase 1 repolarization in normal and failing ventricular myocytes. *J. Mol. Cell Cardiol.* **172**, 52–62, https://doi.org/10.1016/j.yjmcc.2022.07.009

36 Qu, Z., Nivala, M. and Weiss, J.N. (2013) Calcium alternans in cardiac myocytes: order from disorder. *J. Mol. Cell Cardiol.* **58**, 100–109, https://doi.org/10.1016/j.yjmcc.2012.10.007
37 Walker, M.L. and Rosenbaum, D.S. (2005) Cellular alternans as mechanism of cardiac arrhythmogenesis. *Heart Rhythm* **2**, 1383–1386, https://doi.org/10.1016/j.hrthm.2005.09.009
38 Allessie, M.A., Bonke, F.I. and Schopman, F.J. (1977) Circus movement in rabbit atrial muscle as a mechanism of tachycardia. III. The "leading circle" concept: a new model of circus movement in cardiac tissue without the involvement of an anatomical obstacle. *Circ. Res.* **41**, 9–18, https://doi.org/10.1161/01.RES.41.1.9
39 Medeiros-Domingo, A., Bhuiyan, Z.A., Tester, D.J., Hofman, N., Bikker, H., van Tintelen, J.P. et al. (2009) The RYR2-encoded ryanodine receptor/calcium release channel in patients diagnosed previously with either catecholaminergic polymorphic ventricular tachycardia or genotype negative, exercise-induced long QT syndrome: a comprehensive open reading frame mutational analysis. *J. Am. Coll. Cardiol.* **54**, 2065–2074, https://doi.org/10.1016/j.jacc.2009.08.022
40 Greiser, M., Kerfant, B.-G., Williams, G.S.B., Voigt, N., Harks, E., Dibb, K.M. et al. (2014) Tachycardia-induced silencing of subcellular Ca2+ signaling in atrial myocytes. *J. Clin. Invest.* **124**, 4759–4772, https://doi.org/10.1172/JCI70102
41 Lugenbiel, P., Wenz, F., Govorov, K., Schweizer, P.A., Katus, H.A. and Thomas, D. (2015) Atrial fibrillation complicated by heart failure induces distinct remodeling of calcium cycling proteins. *PloS ONE* **10**, e0116395, https://doi.org/10.1371/journal.pone.0116395
42 Briston, S.J., Dibb, K.M., Solaro, R.J., Eisner, D.A. and Trafford, A.W. (2014) Balanced changes in Ca buffering by SERCA and troponin contribute to Ca handling during β-adrenergic stimulation in cardiac myocytes. *Cardiovasc. Res.* **104**, 347–354, https://doi.org/10.1093/cvr/cvu201
43 Chen, W., Wang, R., Chen, B., Zhong, X., Kong, H., Bai, Y. et al. (2014) The ryanodine receptor store-sensing gate controls Ca2+ waves and Ca2+-triggered arrhythmias. *Nat. Med.* **20**, 184–192, https://doi.org/10.1038/nm.3440
44 Künzel, S.R., Hoffmann, M., Weber, S., Künzel, K., Kämmerer, S., Günscht, M. et al. (2021) Diminished PLK2 Induces Cardiac Fibrosis and Promotes Atrial Fibrillation. *Circ. Res.* **129**, 804–820, https://doi.org/10.1161/CIRCRESAHA.121.319425
45 Lv, T., Du, Y., Cao, N., Zhang, S., Gong, Y., Bai, Y. et al. (2016) Proliferation in cardiac fibroblasts induced by β1-adrenoceptor autoantibody and the underlying mechanisms. *Sci. Rep.* **6**, 32430, https://doi.org/10.1038/srep32430
46 Maixent, J.M., Paganelli, F., Scaglione, J. and Lévy, S. (1998) Antibodies against myosin in sera of patients with idiopathic paroxysmal atrial fibrillation. *J. Cardiovasc. Electrophysiol.* **9**, 612–617, https://doi.org/10.1111/j.1540-8167.1998.tb00942.x
47 Stavrakis, S., Yu, X., Patterson, E., Huang, S., Hamlett, S.R., Chalmers, L. et al. (2009) Activating autoantibodies to the beta-1 adrenergic and m2 muscarinic receptors facilitate atrial fibrillation in patients with Graves' hyperthyroidism. *J. Am. Coll. Cardiol.* **54**, 1309–1316, https://doi.org/10.1016/j.jacc.2009.07.015
48 Hindricks, G., Potpara, T., Dagres, N., Arbelo, E., Bax, J.J., Blomström-Lundqvist, C. et al. (2021) 2020 ESC Guidelines for the diagnosis and management of atrial fibrillation developed in collaboration with the European Association for Cardio-Thoracic Surgery (EACTS): The Task Force for the diagnosis and management of atrial fibrillation of the European Society of Cardiology (ESC) Developed with the special contribution of the European Heart Rhythm Association (EHRA) of the ESC. *Eur. Heart J.* **42**, 373–498, https://doi.org/10.1093/eurheartj/ehaa612